Conserved mitochondrial reactive oxygen species and HIF1-alpha signalling during an embryonic critical period directs subsequent nervous system development.

Daniel Sobrido-Cameán[1]*, Bramwell Coulson[2], Matthew C.W. Oswald[1], Tom Pettini[1], Richard A. Baines[2]*, Matthias Landgraf[1]*.

[1]Department of Zoology, University of Cambridge, CB2 3EJ, Cambridge, UK

[2] Division of Neuroscience, School of Biological Sciences, Faculty of Biology, Medicine and Health, University of Manchester, Manchester Academic Health Science Centre, Manchester, M13 9PT, UK

*** Correspondence:**
Corresponding Authors
ds918@cam.ac.uk, ml10006@cam.cam.uk, Richard.Baines@manchester.ac.uk

Keywords: critical period, nervous system, development, *Drosophila melanogaster*, reactive oxygen species, mitochondria, reverse electron transport, HIF 1 alpha, temperature.

Abstract

Developing nervous systems undergo tuning phases, called 'critical periods', during which nerve cells adjust their properties based on their experiences. Thus, robust nervous system function can emerge in the face of the variability that is inherent to the constituent nerve cells; and of unpredictable external influences, notably temperature, that impact on neuronal activity and metabolism. These developmental windows are termed "critical" because neuronal networks display elevated sensitivity and plasticity responses to stimuli, such that disturbances during a critical period, but not outside, can cause lasting mal-adjustment of network function. Though the impact of temperature variations on nervous system development have been well established, the underlying signalling framework remains unknown. To study this, we have harnessed a well-defined critical period of the embryo of the fruit fly, *Drosophila melanogaster*, and asked how heat stress experienced by the embryo leads to lasting changes during subsequent nervous system development, including change to synaptic receptor composition and overgrowth, and altered crawling behaviour. We identified a highly conserved signalling pathway as responsible for this developmental decision window. Heat stress leads to the generation of reactive oxygen species (ROS) within mitochondria by reverse electron transport, at Complex-I of the electron transport chain. This mitochondrial ROS signal is then transmitted to the nucleus by the *Drosophila* homologue of the highly conserved hypoxia inducible factor-1alpha, whose activation during an embryonic critical period, but not outside this sensitive developmental window, induces lasting changes in subsequent development and function of the nervous system.

Introduction

Most animals are not warm blooded and have limited ability to regulate their internal temperature. Therefore, their development is vulnerable to environmental changes in temperature, which affect all biological processes. With respect to the nervous system, variations in developmental temperature can affect cell behaviour and thus the structures and synaptic connectivity that emerge[1]. Insects, such as bees, ants and fruit flies, have a limited capacity to regulate their body temperature, and changes in rearing temperature during pupal development leads to region-specific changes in cell number and connectivity within the developing brain [1–5], with changes in sensory processing, learning and behaviour[1,4–9]. Other poikilothermic animals, amphibians and reptiles, also manifest developmental temperature-dependent variations in behaviour[10,11]. Given the impact that variations in developmental temperature can have on adult learning and other behavioural performance[6–8], it is perhaps not surprising that many social insect have evolved complex behaviours to regulate brood temperature; ranging from nest design to active cooling and heating, including through rhythmic daily movement of pupae to warmer and cooler locations[12].

The changes in brain structure and function, which are caused by temperature experiences during nervous system development, are long lasting. Moreover, specific developmental windows are particularly sensitive to temperature and activity perturbations, and these have therefore been referred to as 'sensitive' or 'critical' periods of development[1,13–16]. The molecular mechanisms by which transient temperature experiences during a critical period of development lead to lasting changes within the nervous system are not known. In this study, we set out to identify those mechanisms, taking advantage of a well-defined critical period of nervous system development in one of the experimentally most tractable model system, the fruit fly, *Drosophila melanogaster*. Specifically, this model system allows genetic manipulations to be targeted to single neurons or muscles during the embryonic critical period, and to thus cell-selectively rescue or mimic the effects of a systemic temperature experience during development.

The locomotor network of the *Drosophila* larva forms during embryonic stages and is particularly sensitive to activity perturbations in late embryonic stages, when the network becomes synaptically active, from 80-90% of development[13–15,17–19]. Activity manipulations during this defined 2-hour critical period, irrespective of whether those increase or decrease network activity, lead to lasting changes in network performance that manifests in reduced crawling speed and network instability[15,19,20]. Nitric oxide signalling has been identified as downstream of neuronal activity, and Baines and co-workers proposed that during a critical period, the overall balance of excitatory and inhibitory activity is integrated by the developing network to shape its properties, and thus its performance and function[21]. A key outcome of critical period adjustments has been suggested to be the specification of network setpoints[15,22]. If correct, this may explain why persisting plasticity mechanisms are often unable to fully correct errors induced by a critical period perturbation. In support, we

found that a critical period heat stress of 32˚C, an ecologically relevant temperature[16], causes a significant reduction in larval crawling speed, compatible with a change of setpoint of the locomotor network[20]. Moreover, transient exposure to 32˚C, when experienced during the embryonic critical period, but not outside this sensitive phase, causes reduction in both neuronal excitability and network stability, thus phenocopying the effects of critical period activity manipulations, as well as changes in neuromuscular junction (NMJ) growth and receptor composition[15,20,21,23].

In addition to affecting neuronal activity, variations in temperature affect biochemical reactions in general, and metabolic and mitochondrial processes in particular[24]. In *Drosophila,* 32˚C causes a reversal of the flow of electrons within the mitochondrial electron transport chain (ETC), from Complex-II back to Complex-I, called reverse electron transport (RET). This leads to the production of reactive oxygen species (ROS) at Complex-I, due to the partial reduction of oxygen and the formation of superoxide anions. In *Drosophila*, as well as mouse, RET-generated ROS have been linked to increased lifespan and improved stress resistance[25–29]. Thus, RET-based generation of ROS at mitochondrial Complex-1 is a candidate signalling pathway by which heat stress during the critical period could cause cellular changes, including to subsequent development.

One of the targets of mitochondrial ROS, which could transduce the mitochondrial signal to the nucleus to promote the expression of genes coding for protective molecules, is the conserved Hypoxia-inducible factor 1 alpha (HIF-1α)[30–32]. HIF-1α is, amongst others, also a sensor for oxygen levels and a regulator of glycolytic enzyme expression[33], whose dysregulation is linked to a range of cancers[34]. During normal development, HIF-1α regulates many processes, including neurogenesis, angiogenesis, and cell survival[35–37]. The molecular mechanisms governing the hypoxia-responsive system are highly conserved, though there is only a single *Drosophila* homologue, called *similar (sima),* but multiple HIFs in mammals. Briefly, HIF-1α signalling is facilitated by transient inhibition of its continual proteasomal degradation. Under normoxic conditions, the conserved prolyl-4-hydroxylase (PHD), named Fatiga in *Drosophila*, marks HIF-1α for recognition by a van-Hippel-Lindau (VHL)-E3 ubiquitin ligase complex[38].

Here, through cell-selective genetic rescue and manipulation experiments, we identified mitochondrial ROS generated by RET as the basic signal that triggers lasting developmental change, when heat stress is experienced during the embryonic critical period. We further show that HIF-1α is a downstream effector, which transduces this mitochondrial signal to the nucleus. Thus, during the embryonic critical period, RET-generated ROS, via HIF-1α signalling, are necessary and sufficient to generate lasting changes in the nervous system, both at the level of peripheral NMJ and the central locomotor network.

Results

Mitochondrial ROS are plasticity signals during the embryonic critical period

To identify the signalling pathways that translate critical period perturbations into lasting change of nervous system development and function, we focused on the *Drosophila* larval NMJ, which has served successfully as an experimental model system for similar undertakings[39–41]. We recently found that a transient heat stress of 32°C, when experienced during the embryonic critical period (17 -19 hr after egg laying), leads to an overgrowth of the presynaptic NMJ terminal by the late larval stage[20] (Figure 1A-C). The postsynaptic muscle is also affected, showing a decrease in postsynaptic high-conductance glutamate receptor subunit, GluRIIA (Figure 1D), while leaving levels of the lower conductance subunit, GluRIIB, unaffected (Figure 1E).

The NMJ overgrowth phenotype resembled outcomes from neuronal overactivation-induced reactive oxygen species (ROS) signalling, which we had previously studied[42,43]. We therefore asked if mitochondrial ROS might be involved. To test this, we genetically manipulated mitochondrial ROS levels in embryonic stages only, selectively within a single muscle per half segment; the most dorsal muscle, dorsal acute 1 (DA1). Mis-expression of the mitochondrially targeted ROS scavenger, mito-Catalase or Perexiredoxin-3 (Prx3), in muscle DA1, cell-selectively rescues the NMJ overgrowth (Figure 1C) and GluRIIA phenotypes that otherwise result from a systemically experienced heat stress during the embryonic critical period (Figure 1D). While at the control temperature of 25°C, no lasting effects result from these transient genetic manipulations (Figure 1).

Mitochondria can generate ROS through various means, notably at Complex-I and Complex-III of the electron transport chain. 32°C heat stress causes ROS generation at Complex-I in adult *Drosophila*, via reverse flow of electrons from Complex-II back to Complex-I, called 'reverse electron transport', or 'RET'[27]. To test if 32°C heat stress in embryos causes RET-generated ROS in mitochondria, we cell-selectively knocked down a subunit of Complex-I, ND-75, instrumental for RET-generated ROS. Complementing, we neutralised RET-generated ROS by mis-expression of alternative oxidase (AOX), an enzyme found in the inner mitochondrial membrane of many organisms including flies[44–47]. In mitochondria, AOX acts as a bypass that transfers electrons from ubiquinone to oxygen, independent of Complexes-I and -III, thereby reducing the probability of electron backflow through these complexes and subsequent ROS production by RET[27,48–50]. When we targeted either of these genetic manipulations to muscle DA1 during embryonic stages, while simultaneously exposing embryos to 32°C heat stress, they rescued the NMJ critical period heat stress phenotype (Figure 1). In contrast, under control conditions of 25°C both manipulations left NMJ development unaffected (Figure 1). Together, these results show that during the embryonic critical period, RET-generated ROS at Complex-I are necessary for heat stress to effect a lasting change in subsequent NMJ development.

Mitochondrial RET-generated ROS are critical period signals that direct NMJ development.

We next asked if ROS generated by Complex-I might be sufficient for inducing lasting changes, in absence of systemic heat stress, which might affect many other aspects of biology. To test this, we cell-selectively induced RET-ROS at Complex-I by mis-expression of NADH dehydrogenase 1 (Ndi1) from yeast. Ndi1 transfers electrons from NADH to the CoQ pool. This can lead to the accumulation of reduced CoQ and transfer of electrons to Complex-I, causing RET and thus generation of ROS at Complex-I. Mis-expression of Ndi1 in *Drosophila* had previously been shown to increase ROS production in a way indistinguishable from RET[28]. Indeed, we found that transient embryonic mis-expression of Ndi1 in muscle DA1, at the control temperature of 25°C, cell-selectively phenocopies the characteristic critical period heat stress phenotype of NMJ overgrowth (Figure 2A-C) and reduced GluRIIA levels (Figure 2E). Thus, our results show that in postsynaptic muscles during the embryonic critical period RET-generated ROS are mitochondrial signals that are both necessary and sufficient for inducing lasting change to NMJ development.

Because synapse development depends on the close interactions between pre- and postsynaptic partners, we next tested the roles of these mitochondrial signals in the presynaptic motoneuron, called 'aCC' , which forms a NMJ terminal on muscle DA1. For this we were fortunate to have a transgenic line that transiently targets Gal4 expression, during embryonic stages only, to the aCC presynaptic motoneuron (plus the co-innervating 'RP2' motoneuron and a single interneuron, 'pCC'). Using this aCC-Gal4 [1] genetic tool (aka RN2-O-Gal4), we found that mis-expression of AOX in the aCC motoneurons, to neutralise RET-induced ROS generation at Complex-I, was sufficient to rescue NMJ overgrowth that normally results from embryonic experience of 32°C heat stress. Transient AOX mis-expression at the control temperature of 25°C, on the other hand, had not effect (Figure 3). Increases in NMJ size led to proportionate increases in the number of presynaptic active zones, the sites of vesicular neurotransmitter release. Active zone number was also fully rescued by simultaneous embryonic mis-expression of AOX in the aCC motoneurons (Figure 3D). Conversely, transient embryonic generation of RET-ROS in the aCC motoneurons by mis-expression of Ndi1, to artificially induce RET and ROS at Complex-I, was sufficient to cell-selectively mimic the critical period heat stress phenotype (Figure 3B-D).

Thus, in embryonic presynaptic motoneurons, as in postsynaptic muscles, mitochondrial ROS generated at Complex-I via RET is instructive in subsequent larval NMJ development. To test the importance of developmental timing during which transient RET-generated ROS can cause such lasting change, we contrasted the effects of transient genetic manipulations of aCC motoneurons, during the late embryonic stage, including the critical period, *versus* after closing of the critical period, during the first larval stage. We achieved temporal and spatial control of Gal4 expression by combining two transgenes. The first is a second, independently generated aCC-Gal4 [2] expression line, *GMR94G06-Gal4*, which specifically targets Gal4 to the aCC motoneuron (and up to two other cells per half neuromere)[51,52].

The second component is a conditional Gal4 inhibitor from the recently published "AGES" system: feeding of auxin induces disinhibition of Gal4 through degradation of the Gal4 inhibitor, Gal80[53]. Feeding auxin to gravid females induced Gal4 activity in the aCC motoneuron from 14 hrs after egg laying, i.e. 3 hours before critical period opening, while for post critical period closing, we fed auxin to freshly hatched larvae for 24 hours. The results confirm that the timing of mitochondrial RET-generated ROS is important: only when cells generate these mitochondrial ROS signals during the embryonic phase, including the critical period, do those ROS cause lasting changes, in keeping with this being a sensitive or critical period of NMJ development (supplementary figure 1).

The conserved HIF-1α pathway transduces the mitochondrial ROS signal to the nucleus.

We next considered how mitochondrial ROS, that are triggered by heat stress, might effect changes to developmental outcomes? HIF-1α is a transcription factor that plays a central role in cellular response to hypoxia and other stresses[54]. Under normoxic conditions, HIF-1α is continuously synthesized and degraded by the proteasome, thus preventing cytoplasmic HIF-1α accumulation and nuclear translocation. Degradation of HIF-1α is regulated via hydroxylation by the conserved prolyl hydroxylase, PHD (a single *Drosophila* homologue, *Hph/fatiga*). Hydroxylation enables binding of the E3 ligase complex substrate recognition subunit, von Hippel-Lindau (VHL), and leads to HIF-1α ubiquitination, followed by proteasomal degradation[54]. Mitochondrial ROS, including RET-generated, can inhibit PHD and thereby stabilize HIF-1α, also under normoxic conditions[31,55–58]. We therefore asked if RET-generated mitochondrial ROS might induce HIF-1α signalling. To test this hypothesis, we first tested whether HIF-1α is required and sufficient during the critical period to induce heat stress-regulated developmental changes at the NMJ. First, we knocked down the single *Drosophila* homology of *HIF-1α*, *sima,* in DA1 muscles while exposing embryos to 32°C during the critical period. This showed that HIF-1α is necessary during this window to cause heat stress-induced changes in NMJ development, namely overgrowth (Figure 4A-C) and a postsynaptic decrease of the GluRIIA receptor subunit (Figure 4D). Conversely, at the control temperature of 25°C, transient embryonic mis-expression of *HIF-1α* in DA1 muscles is also sufficient to mimic those developmental phenotypes (Figure 4). Consolidating the role of HIF-1α signalling, transient embryonic overactivation, via RNAi knockdown in muscle DA1, of either the prolyl hydroxylase, PHD, or the VHL ubiquitin ligase complex substrate recognition subunit, similarly phenocopy the characteristic NMJ phenotype (Figure 4).

To test the working model of HIF-1α signalling being downstream of mitochondrial RET-generated ROS, we used a genetic epistasis experiment: of inducing RET via mis-expression of Ndi1, while simultaneously knocking down HIF-1α. We found that RET induction was unable to induce a change in larval NMJ development when HIF-1α was knocked down (Figure 4). This confirms the working model of information flow from mitochondrial RET-generated ROS to nuclear HIF-1α.

The mitochondrial ROS to HIF-1α signalling axis is necessary and sufficient during the critical period for specifying neuronal excitability and crawling speed.

We had recently found that transient experience of heat stress during the embryonic critical period leaves a lasting impact on the function of the locomotor system. It leads to a significant reduction in larval crawling speed, paralleled within the CNS by a decrease in neuronal excitability[20]. Following up on these observations, we observed that RET-generated ROS and HIF-1α signalling are necessary during the embryonic critical period for these heat stress-induced changes in neuronal excitability. Whole cell patch clamp recordings from aCC motoneurons at the late larval stage showed that embryonic heat stress of 32°C changed neuronal properties, causing a reduction in excitability, while leaving cell size (proxy measure of membrane capacitance) and resting membrane potential unaffected (Figure 5A-D). We find that this effect of critical period heat stress on neuronal excitability experience requires the RET-ROS - HIF-1α signalling axis, because it is blocked when simultaneously neutralising RET-ROS by mis-expression of AOX in the aCC motoneuron during the embryonic exposure of heat stress, but induced by mis-expression of HIF-1α at 25°C (Figure 5A-D). Similarly, for larval crawling behaviour, we also find that critical period heat stress mediates its effect via mitochondrial RET-ROS and HIF-1α signalling, and that both these signals are also sufficient to phenocopy the reduction in crawling speed (Figure 5E), while similar manipulations outside of the critical period do not have lasting impact (supplementary figure 2). We conclude that during the embryonic critical period, mitochondrial RET-generated ROS are instructive signals that are transmitted to the nucleus via the conserved transcriptional regulator, HIF-1α When activated during the embryonic critical period, this signalling pathway directs subsequent neuronal development, leading to changes in synaptic terminal growth, receptor composition, neuronal excitable properties and larval crawling behaviour (Figure 6).

Discussion

Working with a simplified experimental system, we have identified a conserved signalling pathway from mitochondrial RET-generated ROS to HIF-1α, as instructive during a developmental critical period of nervous system and muscle development in *Drosophila*. This provides a first molecular explanation for how heat stress, when experienced during particular phases of development, but not later, can effect a change in the development of network properties, and thus also of animal behaviour. By virtue of targeting genetic manipulations, transiently, to single cells *in vivo*, we were able to demonstrate that critical period responses, at least to heat stress, RET-generated ROS and HIF-1α are fundamentally cell intrinsic.

Environmental cues are integrated during critical periods and direct nervous system development

It has long been known that early life experiences are formative, due to their potential to impart lasting influence on nervous system function. Though critical periods of nervous

system development have been most intensively studied in the context of activity-regulated sensory processing and cortical networks, it is possible that critical periods represent a fundamental process of nervous system development. For example, similar developmental windows of heightened vulnerability to disturbances have been identified also in mammalian locomotor systems[60], as well as in locomotor, visual and olfactory systems of zebrafish[60–64] and several insect species (ants, bees and *Drosophila*[1–5]). Perhaps this should not be surprising, if one views critical periods as adjustment phases that facilitate networks to compensate for the inevitable variability that is inherent in biological systems, while also integrating genetically unpredictable environmental variables, such as seasonal or daily changes in temperature. In fast developing organisms, opening of a critical period correlates with the phase when network activity transitions from unpatterned to patterned activity, and in the case of the locomotor network of the *Drosophila* embryo lasts only two hours[13–15,18,19,65]. In mammalian systems, critical periods are much more drawn out, lasting weeks in mouse and up to several years in humans[66]. Notwithstanding such differences, the neuronal activity-regulated processes that are central to critical periods are remarkably similar across species; from GABAergic signalling during the critical period in zebrafish visual system development[64] to the importance of the overall excitation:inhibition balance in the developing *Drosophila* locomotor network[18,21].

Here, we took advantage of a well-defined 2-hour critical period of the *Drosophila* locomotor network[15,21] to investigate how temperature is integrated as an important environmental cue. Having previously identified 32°C heat stress as an ecologically relevant stimulus that leads to lasting change in subsequent motoneuron development[20], we now identify the basic instructive signal elicited by this heat stress, namely mitochondrial ROS generated at Complex-I via reverse flow of electrons within the electron transport chain. The reasons why heat stress causes the reverse flow of electrons, whether it acts as a biophysical switch or as a result of temperature-induced changes in mitochondrial metabolism, needs to be determined. In mammals, mitochondrial RET-generated ROS has been associated with ageing and to promote expression of protective responses[27,67]. Whether this same signal is also responsible for the responses to developmental heat stress reported in ants[9], bees[3,7,8] or other parts and stages of the developing *Drosophila* nervous system[1,16], remains to be tested. Though we employed a stress signal in this study, to elicit a robust critical period response, temperature operates as a general environmental cue during nervous system development, at least in pokilothermic animals. Contrasting with this study, a cooler, non-stress temperature experience during the pupal critical period of *Drosophila* nervous system development leads to clear cellular effects; of reduced filopodial dynamics and consequent increase in synapse formation with concomitant changes in network connectivity and behaviour[1,5].

Critical period effects at the level of single cells

One of the strengths of the experimental system we exploit here, is that it allows studying critical period biology with single cell resolution *in vivo*. This simplifies establishing clear

cause-effect relationships, which is more difficult with commonly used network-wide manipulations. Through cell-selective genetic manipulations of a single motoneuron or its target muscle we could phenotypically rescue individual cells from systemic heat stress manipulations. Thus, we demonstrated the cell-autonomous necessity of RET-generated mitochondrial ROS and HIF-1α signalling for heat stress-induced critical period plasticity. Conversely, we also showed cell-selective sufficiency of RET-ROS and HIF-1α signalling to phenocopy changes in NMJ development, though only when induced during the transient embryonic critical period, but not afterwards. We thus demonstrated conclusively *in vivo* that individual cells undergo their own, potentially cell type-specific, critical periods.

From a developmental perspective, this implies that different cell types might be integrated into circuitry in a sequential manner, for example based on birth order or maturation speed, thus facilitating more reproducible and robust network assembly. Across a developing nervous system, different regions are known to undergo their respective critical periods in sequence[66], which is mirrored at the cellular level within a given network. A recent study centred on developing mouse neocortex demonstrated the sequential maturation of two principal classes of inhibitory interneurons, and how this process directs network maturation[68].

Conserved mitochondrial-nuclear signalling directs critical period plasticity

Cells integrate internal (e.g. network activity) and external environmental cues (e.g. temperature) during a critical period. The identification of an instructive signal that is intimately linked to mitochondrial metabolism significantly adds to and complements a large body of work that has focused on activity regulated processes[69,70]. How neuronal activity-regulated signalling and mitochondrial metabolism interlink, especially during critical periods of development, will be important to understand. We had previously shown that mitochondrial and NADPH oxidase-generated ROS are required for activity-regulated neuronal plasticity outside the critical period[42,43,71]. Here, we identified a specific source of mitochondrial ROS, namely those generated at Complex-I via RET, which occurs when the coenzyme Q pool is reduced while the proton motif force is elevated[72]. A mitochondrial enzyme that is linked to the redox state of the coenzyme Q pool, dihydroorotate dehydrogenase (DHODH) has been identified as an important regulator of neuronal action potential firing rate, i.e. a determinant of the neuronal homeostatic setpoint[73]. Together with our findings here we speculate that mitochondrial metabolism might be central to critical period plasticity, potentially specifying neuronal homeostatic setpoints, as previously suggested[22].

How might a transient perturbation during a critical period lead to lasting change? HIF-1α, a transcriptional regulator involved in the cellular response to stress, is typically degraded under normal oxygen conditions. The model we propose is that mitochondrial ROS, including those generated by RET, transiently inhibit the degradation of HIF-1α, thus allowing HIF-1α to accumulate and translocate into the nucleus, also under normoxic conditions[31,55–58]. HIF-

1α signalling is a known regulator of changes in cellular metabolism, for example promoting aerobic glycolysis in a range of cancers[74–76], as well as during normal development, when rapid tissue growth is required[35,78,79]. HIF-1α achieves this through a combination of direct regulation of gene expression, notably of metabolic enzymes, and epigenetic modifications, partly executed through histone acetyl transferases that act as co-factors[79–82]. In some forms of cancer, this is thought to create positive feedback loops, from elevated mitochondrial metabolism, to increased ROS production maintaining disinhibition of HIF-1α, which reinforces metabolic drive. It is therefore possible that transient HIF-1α signalling could initiate such metabolic-epigenetic feedback loops that could maintain a change in metabolic state, and thus also of neuronal growth and functional properties.

Materials and Methods

Drosophila rearing and stocks.

Drosophila stocks were kept on standard corn meal medium, at 25°C. For all experiments where crosses were necessary, stocks were selected and combined as a 1:2 ratio of Gal4-line males to UAS-line virgin females. See table 1 for the strains used.

Critical Period manipulations

Temperature manipulations: Embryos were harvested from 0 to 6 hours after egg lay at 25°C. Embryos were then shifted to their respective temperatures in incubators (25°C or 32°C) from for the remaining of embryogenesis. After all animals hatched, all were move back to 25°C till the assay (Figure 7).

Auxin feeding: Auxin (GK2088 1-Naphthaleneacetic acid potassium salt; Glentham) solution was mixed with melted molasses fly medium to achieve 5mM auxin concentration, poured into petri dish plates. For embryonic exposure to auxin, adult flies in mixed-sex laying pots were fed on this food for 48 hours prior to egg collection. For larval exposure, freshly hatched larvae were fed on this food for 24 hours.

Dissections and immunocytochemistry

Flies were allowed to lay eggs on apple-juice agar based medium overnight at 25°C. Larvae were then reared at 25°C on yeast paste, while avoiding over-crowding. Precise staging of the late wandering third instar stage was achieved by: a) checking that a proportion of animals from the same time-restricted egg lay had initiated pupariation; b) larvae had reached a certain size and c) showed gut-clearance of food (yeast paste supplemented with Bromophenol Blue Sodium Salt (Sigma-Aldrich)). Larvae (of either sex) were dissected in Sorensen's saline, fixed for 10 min at room temperature in Bouins fixative (Sigma-Aldrich; as previously detailed[43]. Wash solution was Sorensen's saline containing 0.3% Triton X-100 (Sigma-Aldrich) and 0.25% BSA (Sigma-Aldrich). Primary antibodies, incubated overnight at 10°C, were: Goat-anti-HRP Alexa Fluor 488 (1:1000; Jackson ImmunoResearch Cat. No. 123-545-021), Rabbit-anti-GluRIIB (1:1000; gift from Mihaela Serpe[83]), Mouse anti-GluRIIA (1:100; Developmental Studies Hybridoma Bank, Cat. No. 8B4D2 (MH2B)); secondary antibodies, 2 hr at room temperature: Donkey anti-Mouse StarRed (1:1000; Abberior,

cat.no. STRED-1001); and goat anti-Rabbit Atto594 (1:1000; Sigma-Aldrich Cat No 77671-1ML-F). Specimens were cleared in 80% glycerol, overnight at 4°C, then mounted in Mowiol.

Image acquisition and analysis

Specimens were imaged using an Olympus FV3000 point-scanning confocal, and a 60x/1.3 N.A silicone oil immersion objective lens and FV31S-SW software. Confocal images were processed using ImageJ (to quantify GluRIIA and -B intensity) and Affinity Photo (Adobe; to prepare figures). Bouton number of the NMJ on muscle DA1 from segments A3-A5 was determined by counting every distinct spherical varicosity along the NMJ branch.

To quantify GluRIIA and -B fluorescence intensity a threshold image for each channel was used to generate an outline selection, which included only the postsynaptic glutamate receptor clusters. This outline was then applied to the original image to define the regions of interest for analysis. Fluorescence intensities for GluRIIA and GluRIIB channels was measured within these outlines. Data were exported into Excel and the intensity values normalised to the negative control condition (25°C through all embryogenesis).

Electrophysiology

Third instar (L3) larvae (of either sex) were dissected in a dish containing standard saline (135mM NaCl (Fisher Scientific), 5mM KCl (Fisher Scientific), 4mM $MgCl_2 \cdot 6H_2O$ (Sigma-Aldrich), 2mM $CaCl_2 \cdot 2H_2O$ (Fisher Scientific), 5mM TES (Sigma-Aldrich), 36mM sucrose (Fisher Scientific), pH 7.15) to remove the ventral nerve cord and brain lobes (CNS). The isolated CNS was then transferred to a droplet of external saline containing 200 μM Mecamylamine which was used to block postsynaptic nACh receptors in order to synaptically isolate motor neurons. CNSs were laid flat (dorsal side up) and glued (GLUture Topical Tissue Adhesive; World Precision Instruments USA) to a Sylgard-coated cover slip (1 to 2mm depth of cured SYLGARD Elastomer (Dow-Corning USA) on a 22 x 22mm square coverslip). Preparations were then placed on a glass slide and then under a microscope (Olympus BX51-WI), viewed using a 60x water-immersion lens. To access soma, 1% protease (Streptomyces griseus, Type XIV, Sigma-Aldrich, in external saline) contained within a wide-bore glass pipette (GC100TF-10; Harvard Apparatus UK, approx. 10 μm opening) was applied to abdominal segments, roughly between A5-A2 (Baines and Bate, 1998). This was done to remove overlaying glia to facilitate access to underlying nerve cell soma (e.g., aCC). Motoneurons were identified by anatomical position and relative cell size, with aCC being positioned close to the midline and containing both an ipsilateral and contralateral projection. Whole cell patch clamp recordings were made using borosilicate glass pipettes (GC100F-10, Harvard Apparatus) that were fire polished to resistances of 10 - 15MΩ when filled with intracellular saline (140 mM potassium-D-gluconate (Sigma-Aldrich), 2 mM $MgCl_2 \cdot 6H_2O$ (Sigma-Aldrich), 2 mM EGTA (Sigma-Aldrich), 5 mM KCl (Fisher Scientific), and 20 mM HEPES (Sigma-Aldrich), (pH 7.4). Input resistance was measured in the 'whole cell' configuration, and only cells that had an input resistance ≥ 0.5 GΩ were used for experiments. Cell capacitance and break-in resting membrane potential were

measured for each cell recorded; only cells with a membrane potential upon break in of < -40 mV were analysed. Data for current step recordings was captured using a Multiclamp 700B amplifier (Molecular Devices) controlled by pCLAMP (version 10.7.0.3), via an analogue-to-digital converter (Digidata 1440A, Molecular Devices). Recordings were sampled at 20 kHz and filtered online at 10 kHz. Once patched, neurons were brought to a membrane potential of -60 mV using current injection. Each recording consisted of 20 x 4 pA (500 ms) current steps, including an initial negative step, giving a range of -4 to +72 pA. Number of action potentials were counted and plotted against injected current. Cell capacitance and membrane potential were measured between conditions to ensure that any observed differences in excitability were not due to differences in either cell size or resting state.

Larval crawling analysis

Larvae crawling was recorded at the mid-third instar stage, 72 hours after larval hatching (ALH). Larvae were rinsed in water and placed inside a 24cm x 24cm crawling arena with a base of 5mm thick 0.8% agarose gel (Bacto Agar), situated inside an incubator. Temperature was maintained at 25±0.5°C, reported via a temperature probe in the agar medium. Humidity was kept constant. Larval crawling was recorded using a frustrated total internal reflection-based imaging method (FIM) in conjunction with the tracking software FIMTrack (Risse et al., 2017, 2013) using a Basler acA2040-180km CMOS camera with a 16mm KOWA-IJM3sHC.SW-VIS-NIR Lens controlled by Pylon (by Basler) and Streampix (v.6) software (by NorPix). Larvae were recorded for 20 minutes at five frames per second.

Recordings were split into four 5-minute sections with the first section not tracked and analysed as larvae are acclimatising to the crawling arena. The remaining three sections were used to analyse crawling speed, with each larva sampled at most once per section. Crawling speed was calculated using FIMTrack software choosing crawling tracks that showed periods of uninterrupted forward crawling devoid of pauses, turning or collision events. The distance travelled was determined via the FIMTrack output.

Statistical analysis

Statistical analyses were done using GraphPad Prism Software (Version 10.1.2). Datasets were tested for normal distribution with the Shapiro-Wilk Test. Normally distributed data were then tested with students t-test (for pairwise comparison). Normally distributed analysis for more than two groups was done with a one-way ANOVA and post hoc tested with a Tukey multiple comparison test. Non-normally distributed data sets of two groups were tested with Mann-Whitney U Test (pairwise comparison) and datasets with more than two groups were tested with a Kruskal Wallis ANOVA and post hoc tested with a Dunns multiple post hoc comparison test. For whole cell electrophysiology in aCC neurons, linear regression analysis was used to compare the intercepts between conditions, using a Bonferoni correction for multiple comparisons, resulting in an adjusted significance threshold of $p < 0.0083$. This analysis was restricted to the linear portions of the input-

output curves. For all datasets mean and standard error of mean (SEM) are shown. Significance levels were * $p<0.05$; ** $p<0.01$; *** $p<0.001$; **** $p<0.0001$.

References

1. Kiral, F.R., Dutta, S.B., Linneweber, G.A., Hilgert, S., Poppa, C., Duch, C., Von Kleist, M., Hassan, B.A., and Hiesinger, P.R. (2021). Brain connectivity inversely scales with developmental temperature in Drosophila. Cell Rep. *37*, 110145. https://doi.org/10.1016/j.celrep.2021.110145.

2. Falibene, A., Roces, F., Rössler, W., and Groh, C. (2016). Daily Thermal Fluctuations Experienced by Pupae via Rhythmic Nursing Behavior Increase Numbers of Mushroom Body Microglomeruli in the Adult Ant Brain. Front. Behav. Neurosci. *10*. https://doi.org/10.3389/fnbeh.2016.00073.

3. Groh, C., Tautz, J., and Rössler, W. (2004). Synaptic organization in the adult honey bee brain is influenced by brood-temperature control during pupal development. Proc. Natl. Acad. Sci. *101*, 4268–4273. https://doi.org/10.1073/pnas.0400773101.

4. Wang, G., Gordon, T.N., and Rainwater, S. (2008). Maximum voluntary temperature of insect larvae reveals differences in their thermal biology. J. Therm. Biol. *33*, 380–384. https://doi.org/10.1016/j.jtherbio.2008.06.002.

5. Züfle, P., Batista, L.L., Brandão, S.C., D'Uva, G., Christian, D., and Martelli, C. (2023). Metabolic constraints on growth explain how developmental temperature scales synaptic connectivity relevant for behaviour. Preprint, https://doi.org/10.1101/2023.10.15.562389 https://doi.org/10.1101/2023.10.15.562389.

6. Baleba, S.B.S., Mahadevan, V.P., Knaden, M., and Hansson, B.S. (2023). Temperature-dependent modulation of odor-dependent behavior in three drosophilid fly species of differing thermal preference. Commun. Biol. *6*, 905. https://doi.org/10.1038/s42003-023-05280-5.

7. Becher, M.A., Scharpenberg, H., and Moritz, R.F.A. (2009). Pupal developmental temperature and behavioral specialization of honeybee workers (Apis mellifera L.). J. Comp. Physiol. A *195*, 673–679. https://doi.org/10.1007/s00359-009-0442-7.

8. Tautz, J., Maier, S., Groh, C., Rössler, W., and Brockmann, A. (2003). Behavioral performance in adult honey bees is influenced by the temperature experienced during their pupal development. Proc. Natl. Acad. Sci. *100*, 7343–7347. https://doi.org/10.1073/pnas.1232346100.

9. Weidenmüller, A., Mayr, C., Kleineidam, C.J., and Roces, F. (2009). Preimaginal and Adult Experience Modulates the Thermal Response Behavior of Ants. Curr. Biol. *19*, 1897–1902. https://doi.org/10.1016/j.cub.2009.08.059.

10. Noble, D.W.A., Stenhouse, V., Riley, J.L., Warner, D.A., While, G.M., Du, W.-G., Uller, T., and Schwanz, L.E. (2018). A comprehensive database of thermal developmental plasticity in reptiles. Sci. Data *5*, 180138. https://doi.org/10.1038/sdata.2018.138.

11. Ohmer, M.E.B., Hammond, T.T., Switzer, S., Wantman, T., Bednark, J.G., Paciotta, E., Coscia, J., and Richards-Zawacki, C.L. (2023). Developmental environment has lasting effects on amphibian post-metamorphic behavior and thermal physiology. J. Exp. Biol. *226*, jeb244883. https://doi.org/10.1242/jeb.244883.

12. Jones, J.C., and Oldroyd, B.P. (2006). Nest Thermoregulation in Social Insects. In Advances in Insect Physiology (Elsevier), pp. 153–191. https://doi.org/10.1016/S0065-2806(06)33003-2.

13. Crisp, S., Evers, J.F., Fiala, A., and Bate, M. (2008). The development of motor coordination in *Drosophila* embryos. Development *135*, 3707–3717. https://doi.org/10.1242/dev.026773.

14. Crisp, S.J., Evers, J.F., and Bate, M. (2011). Endogenous Patterns of Activity Are Required for the Maturation of a Motor Network. J. Neurosci. *31*, 10445–10450. https://doi.org/10.1523/JNEUROSCI.0346-11.2011.

15. Giachello, C.N.G., and Baines, R.A. (2015). Inappropriate Neural Activity during a Sensitive Period in Embryogenesis Results in Persistent Seizure-like Behavior. Curr. Biol. *25*, 2964–2968. https://doi.org/10.1016/j.cub.2015.09.040.

16. Williamson, M., Mitchell, A., and Condron, B. (2021). Birth temperature followed by a visual critical period determines cooperative group membership. J. Comp. Physiol. A *207*, 739–746. https://doi.org/10.1007/s00359-021-01512-3.

17. Marley, R., and Baines, R.A. (2011). Increased persistent Na^+ current contributes to seizure in the slamdance bang-sensitive *Drosophila* mutant. J. Neurophysiol. *106*, 18–29. https://doi.org/10.1152/jn.00808.2010.

18. Carreira-Rosario, A., York, R.A., Choi, M., Doe, C.Q., and Clandinin, T.R. (2021). Mechanosensory input during circuit formation shapes Drosophila motor behavior through patterned spontaneous network activity. Curr. Biol. *31*, 5341-5349.e4. https://doi.org/10.1016/j.cub.2021.08.022.

19. Zeng, X., Komanome, Y., Kawasaki, T., Inada, K., Jonaitis, J., Pulver, S.R., Kazama, H., and Nose, A. (2021). An electrically coupled pioneer circuit enables motor development via

proprioceptive feedback in Drosophila embryos. Curr. Biol. *31*, 5327-5340.e5. https://doi.org/10.1016/j.cub.2021.10.005.

20. Krick, N., Davies, J., Coulson, B., Sobrido-Cameán, D., Miller, M., Oswald, M.C.W., Zarin, A.A., Baines, R., and Landgraf, M. (2024). Heterogeneous responses to embryonic critical period perturbations among different components of the *Drosophila* larval locomotor circuit. Preprint, https://doi.org/10.1101/2024.09.14.613036 https://doi.org/10.1101/2024.09.14.613036.

21. Hunter, I., Coulson, B., Pettini, T., Davies, J.J., Parkin, J., Landgraf, M., and Baines, R.A. (2024). Balance of activity during a critical period tunes a developing network. eLife *12*, RP91599. https://doi.org/10.7554/eLife.91599.

22. Truszkowski, T.L.S., and Aizenman, C.D. (2015). Neurobiology: Setting the Set Point for Neural Homeostasis. Curr. Biol. *25*, R1132–R1133. https://doi.org/10.1016/j.cub.2015.10.021.

23. Giachello, C.N.G., Fan, Y.N., Landgraf, M., and Baines, R.A. (2021). Nitric oxide mediates activity-dependent change to synaptic excitation during a critical period in Drosophila. Sci. Rep. *11*, 20286. https://doi.org/10.1038/s41598-021-99868-8.

24. Somero, G.N., Lockwood, B.L., and Tomanek, L. (2017). Biochemical adaptation: response to environmental challenges from life's origins to the Anthropocene (Sinauer associates, Inc. publishers).

25. Scialò, F., Sriram, A., Fernández-Ayala, D., Gubina, N., Lõhmus, M., Nelson, G., Logan, A., Cooper, H.M., Navas, P., Enríquez, J.A., et al. (2016). Mitochondrial ROS Produced via Reverse Electron Transport Extend Animal Lifespan. Cell Metab. *23*, 725–734. https://doi.org/10.1016/j.cmet.2016.03.009.

26. Scialò, F., Fernández-Ayala, D.J., and Sanz, A. (2017). Role of Mitochondrial Reverse Electron Transport in ROS Signaling: Potential Roles in Health and Disease. Front. Physiol. *8*, 428. https://doi.org/10.3389/fphys.2017.00428.

27. Scialò, F., Sriram, A., Stefanatos, R., Spriggs, R.V., Loh, S.H.Y., Martins, L.M., and Sanz, A. (2020). Mitochondrial complex I derived ROS regulate stress adaptation in Drosophila melanogaster. Redox Biol. *32*, 101450. https://doi.org/10.1016/j.redox.2020.101450.

28. Sanz, A., Soikkeli, M., Portero-Otín, M., Wilson, A., Kemppainen, E., McIlroy, G., Ellilä, S., Kemppainen, K.K., Tuomela, T., Lakanmaa, M., et al. (2010). Expression of the yeast NADH dehydrogenase Ndi1 in *Drosophila* confers increased lifespan independently of dietary restriction. Proc. Natl. Acad. Sci. *107*, 9105–9110. https://doi.org/10.1073/pnas.0911539107.

29. Sanz, A., Stefanatos, R., and McIlroy, G. (2010). Production of reactive oxygen species by the mitochondrial electron transport chain in Drosophila melanogaster. J. Bioenerg. Biomembr. *42*, 135–142. https://doi.org/10.1007/s10863-010-9281-z.

30. Chandel, N.S., McClintock, D.S., Feliciano, C.E., Wood, T.M., Melendez, J.A., Rodriguez, A.M., and Schumacker, P.T. (2000). Reactive Oxygen Species Generated at Mitochondrial Complex III Stabilize Hypoxia-inducible Factor-1α during Hypoxia. J. Biol. Chem. *275*, 25130–25138. https://doi.org/10.1074/jbc.M001914200.

31. Movafagh, S., Crook, S., and Vo, K. (2015). Regulation of Hypoxia-Inducible Factor-1a by Reactive Oxygen Species: New Developments in an Old Debate: Regulation of Hypoxia-Inducible Factor-1a. J. Cell. Biochem. *116*, 696–703. https://doi.org/10.1002/jcb.25074.

32. Qutub, A.A., and Popel, A.S. (2008). Reactive Oxygen Species Regulate Hypoxia-Inducible Factor 1α Differentially in Cancer and Ischemia. Mol. Cell. Biol. *28*, 5106–5119. https://doi.org/10.1128/MCB.00060-08.

33. Huang, X., Zhao, L., and Peng, R. (2022). Hypoxia-Inducible Factor 1 and Mitochondria: An Intimate Connection. Biomolecules *13*, 50. https://doi.org/10.3390/biom13010050.

34. Iacobini, C., Vitale, M., Pugliese, G., and Menini, S. (2023). The "sweet" path to cancer: focus on cellular glucose metabolism. Front. Oncol. *13*, 1202093. https://doi.org/10.3389/fonc.2023.1202093.

35. Tomita, S., Ueno, M., Sakamoto, M., Kitahama, Y., Ueki, M., Maekawa, N., Sakamoto, H., Gassmann, M., Kageyama, R., Ueda, N., et al. (2003). Defective Brain Development in Mice Lacking the *Hif-1* α Gene in Neural Cells. Mol. Cell. Biol. *23*, 6739–6749. https://doi.org/10.1128/MCB.23.19.6739-6749.2003.

36. Semenza, G.L. (2006). Regulation of physiological responses to continuous and intermittent hypoxia by hypoxia-inducible factor 1. Exp. Physiol. *91*, 803–806. https://doi.org/10.1113/expphysiol.2006.033498.

37. Milosevic, J., Maisel, M., Wegner, F., Leuchtenberger, J., Wenger, R.H., Gerlach, M., Storch, A., and Schwarz, J. (2007). Lack of Hypoxia-Inducible Factor-1α Impairs Midbrain Neural Precursor Cells Involving Vascular Endothelial Growth Factor Signaling. J. Neurosci. *27*, 412–421. https://doi.org/10.1523/JNEUROSCI.2482-06.2007.

38. Yu, F., White, S.B., Zhao, Q., and Lee, F.S. (2001). HIF-1α binding to VHL is regulated by stimulus-sensitive proline hydroxylation. Proc. Natl. Acad. Sci. *98*, 9630–9635. https://doi.org/10.1073/pnas.181341498.

39. Collins, C.A., Wairkar, Y.P., Johnson, S.L., and DiAntonio, A. (2006). Highwire Restrains Synaptic Growth by Attenuating a MAP Kinase Signal. Neuron *51*, 57–69. https://doi.org/10.1016/j.neuron.2006.05.026.

40. Shen, W., and Ganetzky, B. (2009). Autophagy promotes synapse development in *Drosophila*. J. Cell Biol. *187*, 71–79. https://doi.org/10.1083/jcb.200907109.

41. Frank, C.A., Wang, X., Collins, C.A., Rodal, A.A., Yuan, Q., Verstreken, P., and Dickman, D.K. (2013). New Approaches for Studying Synaptic Development, Function, and Plasticity Using *Drosophila* as a Model System. J. Neurosci. *33*, 17560–17568. https://doi.org/10.1523/JNEUROSCI.3261-13.2013.

42. Oswald, M.C., Brooks, P.S., Zwart, M.F., Mukherjee, A., West, R.J., Giachello, C.N., Morarach, K., Baines, R.A., Sweeney, S.T., and Landgraf, M. (2018). Reactive oxygen species regulate activity-dependent neuronal plasticity in Drosophila. eLife *7*, e39393. https://doi.org/10.7554/eLife.39393.

43. Sobrido-Cameán, D., Oswald, M.C.W., Bailey, D.M.D., Mukherjee, A., and Landgraf, M. (2023). Activity-regulated growth of motoneurons at the neuromuscular junction is mediated by NADPH oxidases. Front. Cell. Neurosci. *16*, 1106593. https://doi.org/10.3389/fncel.2022.1106593.

44. McDonald, A.E., and Vanlerberghe, G.C. (2004). Branched Mitochondrial Electron Transport in the Animalia: Presence of Alternative Oxidase in Several Animal Phyla. IUBMB Life *56*, 333–341. https://doi.org/10.1080/1521-6540400000876.

45. McDonald, A.E., Vanlerberghe, G.C., and Staples, J.F. (2009). Alternative oxidase in animals: unique characteristics and taxonomic distribution. J. Exp. Biol. *212*, 2627–2634. https://doi.org/10.1242/jeb.032151.

46. Matus-Ortega, M.G., Salmerón-Santiago, K.G., Flores-Herrera, O., Guerra-Sánchez, G., Martínez, F., Rendón, J.L., and Pardo, J.P. (2011). The alternative NADH dehydrogenase is present in mitochondria of some animal taxa. Comp. Biochem. Physiol. Part D Genomics Proteomics *6*, 256–263. https://doi.org/10.1016/j.cbd.2011.05.002.

47. Weaver, R.J., and McDonald, A.E. (2023). Mitochondrial alternative oxidase across the tree of life: Presence, absence, and putative cases of lateral gene transfer. Biochim. Biophys. Acta BBA - Bioenerg. *1864*, 149003. https://doi.org/10.1016/j.bbabio.2023.149003.

48. Maxwell, D.P., Wang, Y., and McIntosh, L. (1999). The alternative oxidase lowers mitochondrial reactive oxygen production in plant cells. Proc. Natl. Acad. Sci. *96*, 8271–8276. https://doi.org/10.1073/pnas.96.14.8271.

49. Fernandez-Ayala, D.J.M., Sanz, A., Vartiainen, S., Kemppainen, K.K., Babusiak, M., Mustalahti, E., Costa, R., Tuomela, T., Zeviani, M., Chung, J., et al. (2009). Expression of the Ciona intestinalis Alternative Oxidase (AOX) in Drosophila Complements Defects in Mitochondrial Oxidative Phosphorylation. Cell Metab. *9*, 449–460. https://doi.org/10.1016/j.cmet.2009.03.004.

50. El-Khoury, R., Dufour, E., Rak, M., Ramanantsoa, N., Grandchamp, N., Csaba, Z., Duvillié, B., Bénit, P., Gallego, J., Gressens, P., et al. (2013). Alternative Oxidase Expression in the Mouse Enables Bypassing Cytochrome c Oxidase Blockade and Limits Mitochondrial ROS Overproduction. PLoS Genet. *9*, e1003182. https://doi.org/10.1371/journal.pgen.1003182.

51. Pfeiffer, B.D., Jenett, A., Hammonds, A.S., Ngo, T.-T.B., Misra, S., Murphy, C., Scully, A., Carlson, J.W., Wan, K.H., Laverty, T.R., et al. (2008). Tools for neuroanatomy and neurogenetics in *Drosophila*. Proc. Natl. Acad. Sci. *105*, 9715–9720. https://doi.org/10.1073/pnas.0803697105.

52. Liu, K., Jones, S., Minis, A., Rodriguez, J., Molina, H., and Steller, H. (2019). Pl31 Is an Adaptor Protein for Proteasome Transport in Axons and Required for Synaptic Development. Dev. Cell *50*, 509-524.e10. https://doi.org/10.1016/j.devcel.2019.06.009.

53. McClure, C.D., Hassan, A., Aughey, G.N., Butt, K., Estacio-Gómez, A., Duggal, A., Ying Sia, C., Barber, A.F., and Southall, T.D. (2022). An auxin-inducible, GAL4-compatible, gene expression system for Drosophila. eLife *11*, e67598. https://doi.org/10.7554/eLife.67598.

54. Weidemann, A., and Johnson, R.S. (2008). Biology of HIF-1α. Cell Death Differ. *15*, 621–627. https://doi.org/10.1038/cdd.2008.12.

55. Strowitzki, M., Cummins, E., and Taylor, C. (2019). Protein Hydroxylation by Hypoxia-Inducible Factor (HIF) Hydroxylases: Unique or Ubiquitous? Cells *8*, 384. https://doi.org/10.3390/cells8050384.

56. Chandel, N.S., Maltepe, E., Goldwasser, E., Mathieu, C.E., Simon, M.C., and Schumacker, P.T. (1998). Mitochondrial reactive oxygen species trigger hypoxia-induced transcription. Proc. Natl. Acad. Sci. *95*, 11715–11720. https://doi.org/10.1073/pnas.95.20.11715.

57. Brunelle, J.K., Bell, E.L., Quesada, N.M., Vercauteren, K., Tiranti, V., Zeviani, M., Scarpulla, R.C., and Chandel, N.S. (2005). Oxygen sensing requires mitochondrial ROS but not oxidative phosphorylation. Cell Metab. *1*, 409–414. https://doi.org/10.1016/j.cmet.2005.05.002.

58. Guzy, R.D., Hoyos, B., Robin, E., Chen, H., Liu, L., Mansfield, K.D., Simon, M.C., Hammerling, U., and Schumacker, P.T. (2005). Mitochondrial complex III is required for hypoxia-induced ROS production and cellular oxygen sensing. Cell Metab. *1*, 401–408. https://doi.org/10.1016/j.cmet.2005.05.001.

59. Fuhrmann, D.C., and Brüne, B. (2017). Mitochondrial composition and function under the control of hypoxia. Redox Biol. *12*, 208–215. https://doi.org/10.1016/j.redox.2017.02.012.

60. Walton, K.D., Lieberman, D., Llinás, A., Begin, M., and Llinás, R.R. (1992). Identification of a critical period for motor development in neonatal rats. Neuroscience *51*, 763–767. https://doi.org/10.1016/0306-4522(92)90517-6.

61. Moorman, S.J., Cordova, R., and Davies, S.A. (2002). A critical period for functional vestibular development in zebrafish. Dev. Dyn. *223*, 285–291. https://doi.org/10.1002/dvdy.10052.

62. Avitan, L., Pujic, Z., Mölter, J., Van De Poll, M., Sun, B., Teng, H., Amor, R., Scott, E.K., and Goodhill, G.J. (2017). Spontaneous Activity in the Zebrafish Tectum Reorganizes over Development and Is Influenced by Visual Experience. Curr. Biol. *27*, 2407-2419.e4. https://doi.org/10.1016/j.cub.2017.06.056.

63. Xie, J., Jusuf, P.R., Bui, B.V., and Goodbourn, P.T. (2019). Experience-dependent development of visual sensitivity in larval zebrafish. Sci. Rep. *9*, 18931. https://doi.org/10.1038/s41598-019-54958-6.

64. Chin, J.S.R., Phan, T.-A.N., Albert, L.T., Keene, A.C., and Duboué, E.R. (2022). Long lasting anxiety following early life stress is dependent on glucocorticoid signaling in zebrafish. Sci. Rep. *12*, 12826. https://doi.org/10.1038/s41598-022-16257-5.

65. Hageter, J., Starkey, J., and Horstick, E.J. (2023). Thalamic regulation of a visual critical period and motor behavior. Cell Rep. *42*, 112287. https://doi.org/10.1016/j.celrep.2023.112287.

66. Coulson, B., Hunter, I., Doran, S., Parkin, J., Landgraf, M., and Baines, R.A. (2022). Critical periods in Drosophila neural network development: Importance to network tuning and therapeutic potential. Front. Physiol. *13*, 1073307. https://doi.org/10.3389/fphys.2022.1073307.

67. Reh, R.K., Dias, B.G., Nelson, C.A., Kaufer, D., Werker, J.F., Kolb, B., Levine, J.D., and Hensch, T.K. (2020). Critical period regulation across multiple timescales. Proc. Natl. Acad. Sci. *117*, 23242–23251. https://doi.org/10.1073/pnas.1820836117.

68. Graham, C., Stefanatos, R., Yek, A.E.H., Spriggs, R.V., Loh, S.H.Y., Uribe, A.H., Zhang, T., Martins, L.M., Maddocks, O.D.K., Scialo, F., et al. (2022). Mitochondrial ROS signalling

requires uninterrupted electron flow and is lost during ageing in flies. GeroScience. https://doi.org/10.1007/s11357-022-00555-x.

69. Mòdol, L., Moissidis, M., Selten, M., Oozeer, F., and Marín, O. (2024). Somatostatin interneurons control the timing of developmental desynchronization in cortical networks. Neuron *112*, 2015-2030.e5. https://doi.org/10.1016/j.neuron.2024.03.014.

70. Hensch, T.K. (2004). CRITICAL PERIOD REGULATION. Annu. Rev. Neurosci. *27*, 549–579. https://doi.org/10.1146/annurev.neuro.27.070203.144327.

71. Hensch, T.K. (2005). Critical period plasticity in local cortical circuits. Nat. Rev. Neurosci. *6*, 877–888. https://doi.org/10.1038/nrn1787.

72. Dhawan, S., Myers, P., Bailey, D.M.D., Ostrovsky, A.D., Evers, J.F., and Landgraf, M. (2021). Reactive Oxygen Species Mediate Activity-Regulated Dendritic Plasticity Through NADPH Oxidase and Aquaporin Regulation. Front. Cell. Neurosci. *15*, 641802. https://doi.org/10.3389/fncel.2021.641802.

73. Robb, E.L., Hall, A.R., Prime, T.A., Eaton, S., Szibor, M., Viscomi, C., James, A.M., and Murphy, M.P. (2018). Control of mitochondrial superoxide production by reverse electron transport at complex I. J. Biol. Chem. *293*, 9869–9879. https://doi.org/10.1074/jbc.RA118.003647.

74. Styr, B., Gonen, N., Zarhin, D., Ruggiero, A., Atsmon, R., Gazit, N., Braun, G., Frere, S., Vertkin, I., Shapira, I., et al. (2019). Mitochondrial Regulation of the Hippocampal Firing Rate Set Point and Seizure Susceptibility. Neuron *102*, 1009-1024.e8. https://doi.org/10.1016/j.neuron.2019.03.045.

75. Vander Heiden, M.G., Cantley, L.C., and Thompson, C.B. (2009). Understanding the Warburg Effect: The Metabolic Requirements of Cell Proliferation. Science *324*, 1029–1033. https://doi.org/10.1126/science.1160809.

76. Wang, C.-W., Purkayastha, A., Jones, K.T., Thaker, S.K., and Banerjee, U. (2016). In vivo genetic dissection of tumor growth and the Warburg effect. eLife *5*, e18126. https://doi.org/10.7554/eLife.18126.

77. Elzakra, N., and Kim, Y. (2021). HIF-1α Metabolic Pathways in Human Cancer. In Cancer Metabolomics Advances in Experimental Medicine and Biology., S. Hu, ed. (Springer International Publishing), pp. 243–260. https://doi.org/10.1007/978-3-030-51652-9_17.

78. Dunwoodie, S.L. (2009). The Role of Hypoxia in Development of the Mammalian Embryo. Dev. Cell *17*, 755–773. https://doi.org/10.1016/j.devcel.2009.11.008.

79. Bohuslavova, R., Cerychova, R., Papousek, F., Olejnickova, V., Bartos, M., Görlach, A., Kolar, F., Sedmera, D., Semenza, G.L., and Pavlinkova, G. (2019). HIF-1α is required for

development of the sympathetic nervous system. Proc. Natl. Acad. Sci. *116*, 13414–13423. https://doi.org/10.1073/pnas.1903510116.

80. Kallio, P.J. (1998). Signal transduction in hypoxic cells: inducible nuclear translocation and recruitment of the CBP/p300 coactivator by the hypoxia-inducible factor-1alpha. EMBO J. *17*, 6573–6586. https://doi.org/10.1093/emboj/17.22.6573.

81. Perez-Perri, J.I., Dengler, V.L., Audetat, K.A., Pandey, A., Bonner, E.A., Urh, M., Mendez, J., Daniels, D.L., Wappner, P., Galbraith, M.D., et al. (2016). The TIP60 Complex is a Conserved Coactivator of HIF1A. Cell Rep. *16*, 37–47. https://doi.org/10.1016/j.celrep.2016.05.082.

82. Luo, W., and Wang, Y. (2018). Epigenetic regulators: multifunctional proteins modulating hypoxia-inducible factor-α protein stability and activity. Cell. Mol. Life Sci. *75*, 1043–1056. https://doi.org/10.1007/s00018-017-2684-9.

83. Yfantis, A., Mylonis, I., Chachami, G., Nikolaidis, M., Amoutzias, G.D., Paraskeva, E., and Simos, G. (2023). Transcriptional Response to Hypoxia: The Role of HIF-1-Associated Co-Regulators. Cells *12*, 798. https://doi.org/10.3390/cells12050798.

84. Sulkowski, M.J., Han, T.H., Ott, C., Wang, Q., Verheyen, E.M., Lippincott-Schwartz, J., and Serpe, M. (2016). A Novel, Noncanonical BMP Pathway Modulates Synapse Maturation at the Drosophila Neuromuscular Junction. PLOS Genet. *12*, e1005810. https://doi.org/10.1371/journal.pgen.1005810.

Figures

Figure 1. Mitochondrial ROS generated by reverse electron transport are necessary in muscles for critical period heat stress to change NMJ development.

A) Experimental paradigm

B) Representative images of aCC NMJ terminals on muscles DA1 in late wandering third instar larvae (100 hrs after larval hatching). Left: showing neuronal membrane, visualized with anti-HRP; centre: GluRIIA subunit; right: GluRIIB subunit, both displayed with lookup table "fire" to illustrate signal intensities (warmer colours indicating greater signal intensities). Temperature experienced during the embryonic critical period (25°C control *vs* 32°C heat stress) and simultaneous genetic manipulation of muscle DA1 during embryonic stages only. "Control" indicates control genotype heterozygous for Oregon-R and DA1-Gal4. Larvae were reared at the control temperature of 25°C until the late wandering stage, c. 100 hrs ALH Scale bar = 20 μm.

C) Dot-plot quantification shows changes to aCC NMJ growth on its target muscle DA1, based on the standard measure of the number of boutons (swellings containing multiple presynaptic release sites/active zones). Data are show with mean ± SEM, ANOVA, *** $p<0.0001$, **** $p<0.00001$, 'ns' indicates statistical non-significance. Black asterisks indicate comparison with the control condition of 25°C throughout, genetically unmanipulated. Red asterisks indicate comparisons with control genotype exposed to 32°C heat stress during the embryonic critical period.

D) Dot-plot quantification shows changes in levels of the GluRIIA receptor subunit at aCC NMJs quantified in C). Data are shown with mean ± SEM, ANOVA, **** $p<0.00001$, 'ns' indicates statistical non-significance. Black asterisks indicate comparison with the control condition of 25°C throughout, genetically unmanipulated. Red asterisks indicate comparisons with control genotype exposed to 32°C heat stress during the embryonic critical period.

E) Dot-plot quantification as in D), but for the low conductance GluRIIB receptor subunit, which remains unaffected by these manipulations.

A

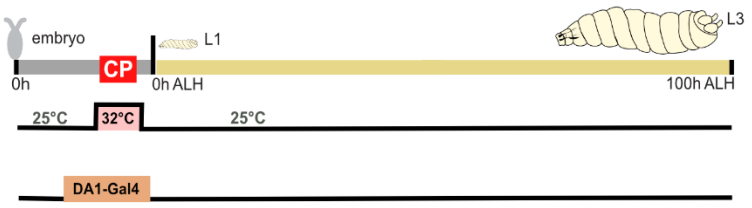
embryo
L1
L3
CP
0h
0h ALH
100h ALH
25°C
32°C
25°C
DA1-Gal4

B

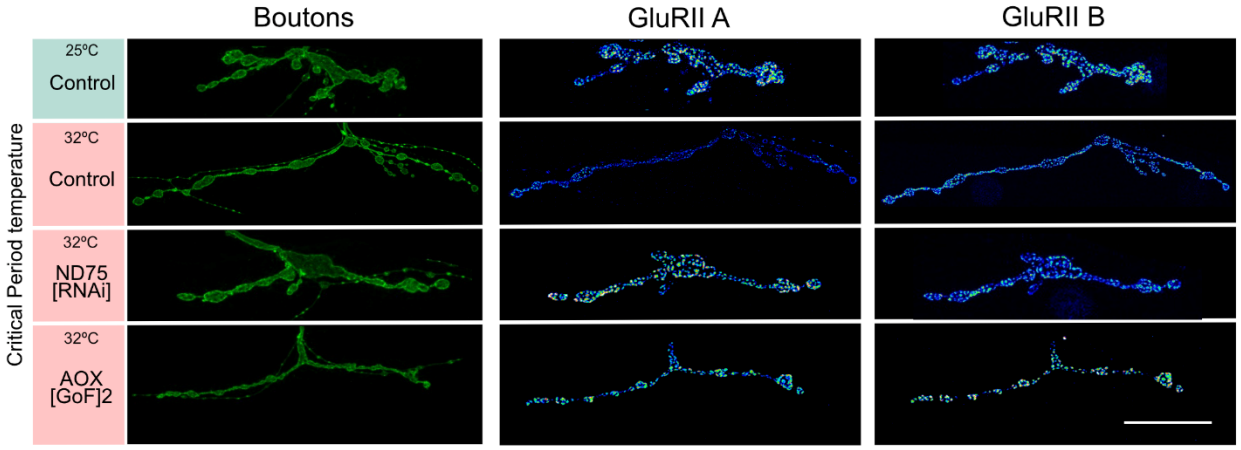
Boutons
GluRII A
GluRII B
Critical Period temperature
25°C
Control
32°C
Control
32°C
ND75 [RNAi]
32°C
AOX [GoF]2

C

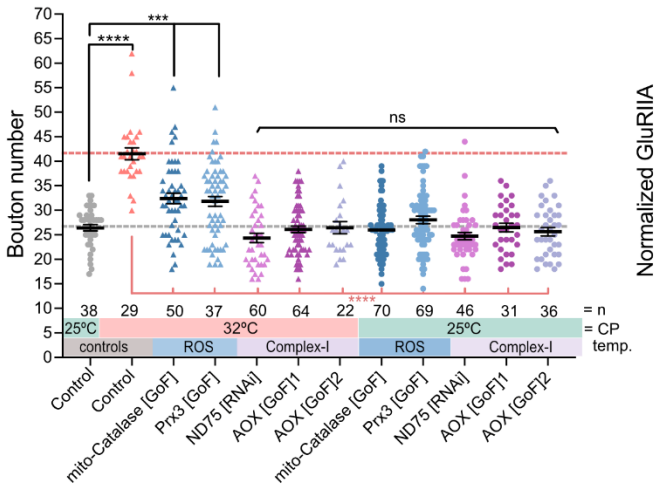
Bouton number
***
****
ns
****
38 29 50 37 60 64 22 70 69 46 31 36 = n
25°C 32°C 25°C = CP temp.
controls ROS Complex-I ROS Complex-I
Control
Control
mito-Catalase [GoF]
Prx3 [GoF]
ND75 [RNAi]
AOX [GoF]1
AOX [GoF]2
mito-Catalase [GoF]
Prx3 [GoF]
ND75 [RNAi]
AOX [GoF]1
AOX [GoF]2

D

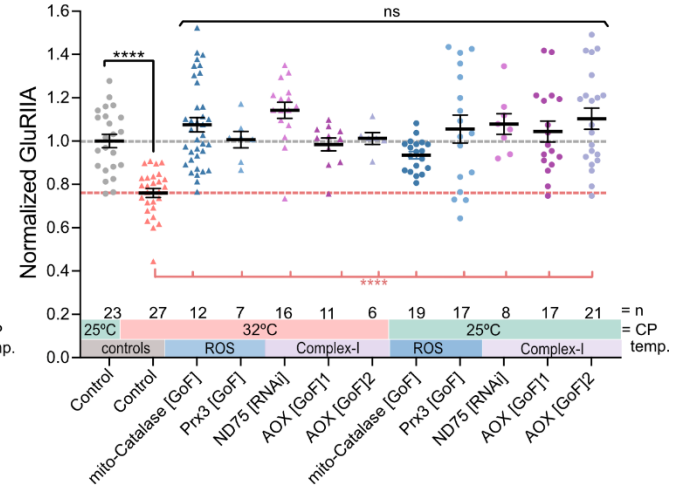
Normalized GluRIIA
ns
****
****
23 27 12 7 16 11 6 19 17 8 17 21 = n
25°C 32°C 25°C = CP temp.
controls ROS Complex-I ROS Complex-I
Control
Control
mito-Catalase [GoF]
Prx3 [GoF]
ND75 [RNAi]
AOX [GoF]1
AOX [GoF]2
mito-Catalase [GoF]
Prx3 [GoF]
ND75 [RNAi]
AOX [GoF]1
AOX [GoF]2

E

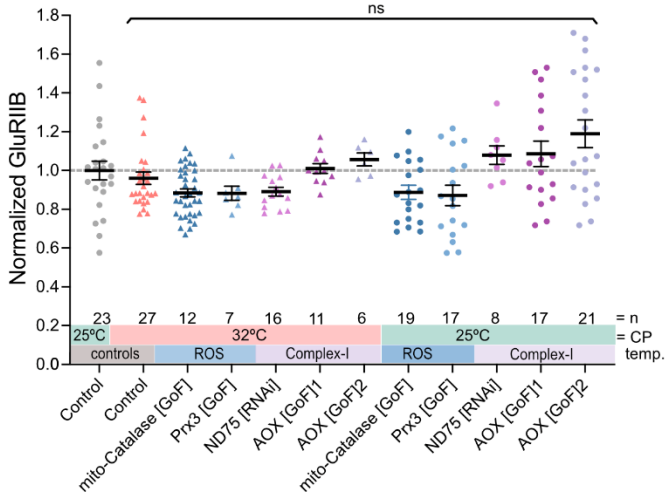
Normalized GluRIIB
ns
23 27 12 7 16 11 6 19 17 8 17 21 = n
25°C 32°C 25°C = CP temp.
controls ROS Complex-I ROS Complex-I
Control
Control
mito-Catalase [GoF]
Prx3 [GoF]
ND75 [RNAi]
AOX [GoF]1
AOX [GoF]2
mito-Catalase [GoF]
Prx3 [GoF]
ND75 [RNAi]
AOX [GoF]1
AOX [GoF]2

Figure 2: ROS by Complex I, during the critical period, are sufficient to induce lasting changes to NMJ development.

A) Experimental paradigm

B) Representative images of aCC NMJ terminals on muscles DA1 in late wandering third instar larvae (100 hrs after larval hatching). Left: showing neuronal membrane, visualized with anti-HRP; centre: GluRIIA subunit; right: GluRIIB subunit, both displayed with lookup table "fire" to illustrate signal intensities (warmer colours indicating greater signal intensities). Temperature experienced during the embryonic critical period (25°C control *vs* 32°C heat stress) and simultaneous genetic manipulation of embryonic muscle DA1 during embryonic stages only. "Control" indicates control genotype heterozygous for Oregon-R and DA1-Gal4. Larvae were reared at the control temperature of 25°C until the late wandering stage, c. 100 hrs ALH Scale bar = 20 μm.

C) Dot-plot quantification shows changes to aCC NMJ growth on its target muscle DA1, based on the standard measure of the number of boutons (swellings containing multiple presynaptic release sites/active zones). Data are show with mean ± SEM, ANOVA, *** $p<0.0001$, **** $p<0.00001$. Black asterisks indicate comparison with the control condition of 25°C throughout, genetically unmanipulated. Red asterisks indicate comparisons with control genotype exposed to 32°C heat stress during the embryonic critical period.

D) Dot-plot quantification shows changes in levels of the GluRIIA receptor subunit at aCC NMJs quantified in C). Data are shown with mean ± SEM, ANOVA, ** $p<0.001$, *** $p<0.0001$, 'ns' indicates statistical non-significance. Black asterisks indicate comparison with the control condition of 25°C throughout, genetically unmanipulated. Red asterisks indicate comparisons with control genotype exposed to 32°C heat stress during the embryonic critical period.

E) Dot-plot quantification as in D), but for the low conductance GluRIIB receptor subunit, which remains unaffected by these manipulations.

A

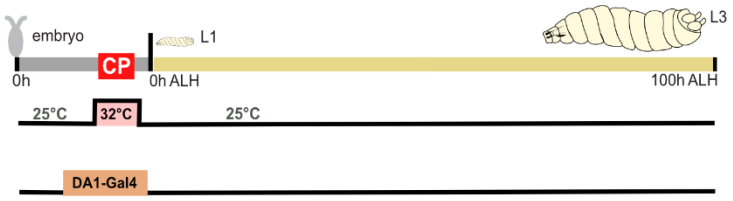
embryo
L1
L3
CP
0h
0h ALH
100h ALH
25°C
32°C
25°C
DA1-Gal4

B

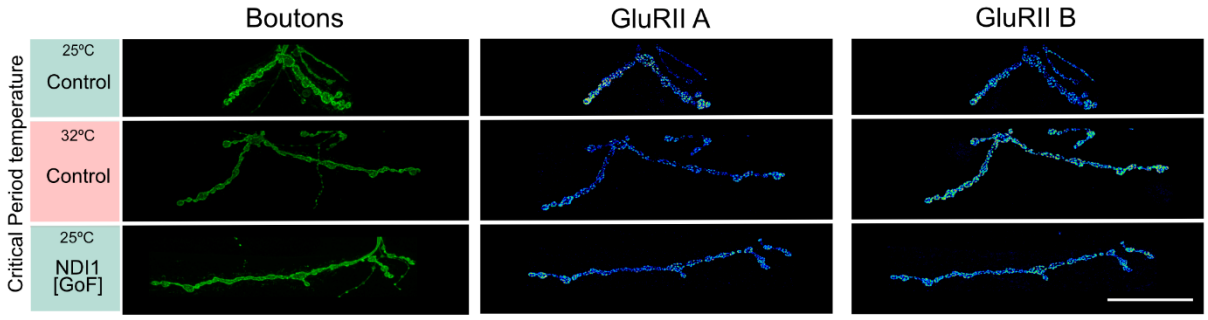
Boutons
GluRII A
GluRII B
Critical Period temperature
25ºC
Control
32ºC
Control
25ºC
NDI1
[GoF]

C

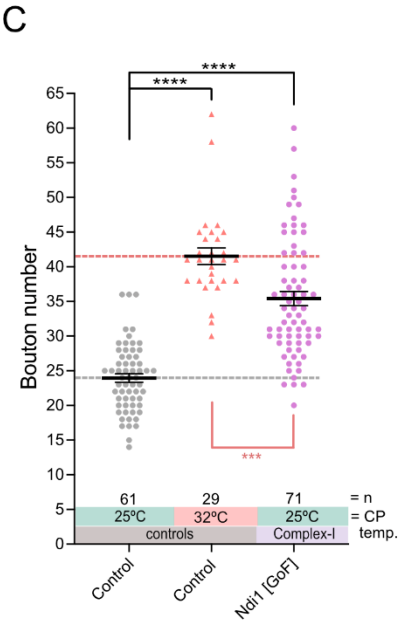
Bouton number
****
****
***
61
29
71
= n
25ºC
32ºC
25ºC
= CP
controls
Complex-I
temp.
Control
Control
Ndi1 [GoF]

D

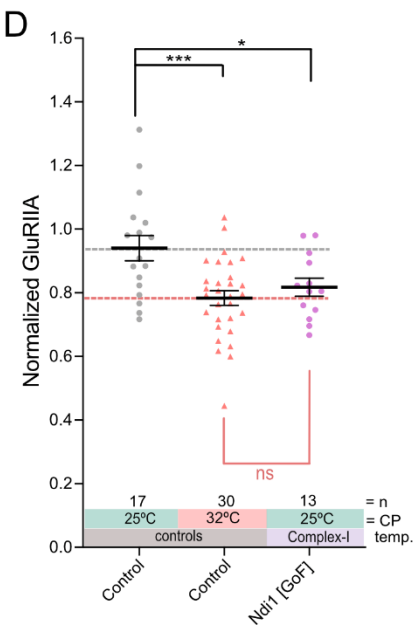
Normalized GluRIIA
***
*
ns
17
30
13
= n
25ºC
32ºC
25ºC
= CP
controls
Complex-I
temp.
Control
Control
Ndi1 [GoF]

E

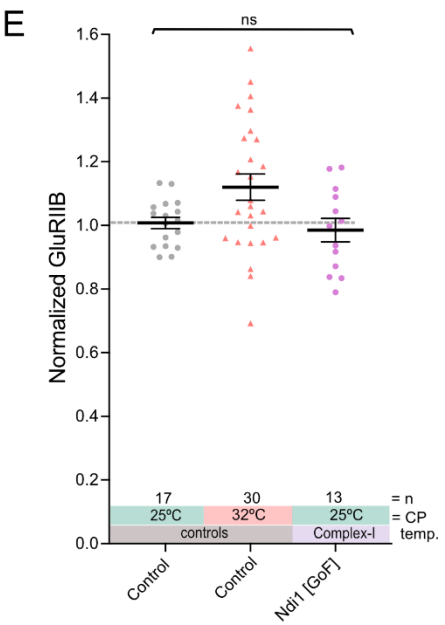
Normalized GluRIIB
ns
17
30
13
= n
25ºC
32ºC
25ºC
= CP
controls
Complex-I
temp.
Control
Control
Ndi1 [GoF]

Figure 3: ROS by RET also signal in motoneurons during the embryonic CP, instructing subsequent NMJ development

A) Experimental paradigm

B) Representative images of aCC NMJ terminals on muscles DA1 in late wandering third instar larvae (100 hrs after larval hatching). Left: showing neuronal membrane, visualized with anti-HRP; right: active zones (α-BRP staining). Temperature experienced during the embryonic critical period (25°C control *vs* 32°C heat stress) and simultaneous, transient genetic manipulation of motoneuron aCC during embryonic stages only via aCC-Gal4 [1] (aka*RN2-O-Gal4*). "Control" indicates control genotype heterozygous for Oregon-R and aCC-Gal4[1]. Larvae were reared at the control temperature of 25°C until the late wandering stage, c. 100 hrs ALH. Scale bar = 20 μm.

C) Dot-plot quantification shows changes to aCC NMJ growth on its target muscle DA1, based on the standard measure of the number of boutons (swellings containing multiple presynaptic release sites/active zones). Data are show with mean ± SEM, ANOVA, **** $p<0.00001$, 'ns' indicates statistical non-significance. Black asterisks indicate comparison with the control condition of 25°C throughout, genetically unmanipulated. Red asterisks indicate comparisons with control genotype exposed to 32°C heat stress during the embryonic critical period.

D) Dot-plot quantification shows changes in number of the active zones at aCC NMJs quantified in C). Data are shown with mean ± SEM, ANOVA, **** $p<0.00001$, 'ns' indicates statistical non-significance. Black asterisks indicate comparison with the control condition of 25°C throughout, genetically unmanipulated. Red asterisks indicate comparisons with control genotype exposed to 32°C heat stress during the embryonic critical period.

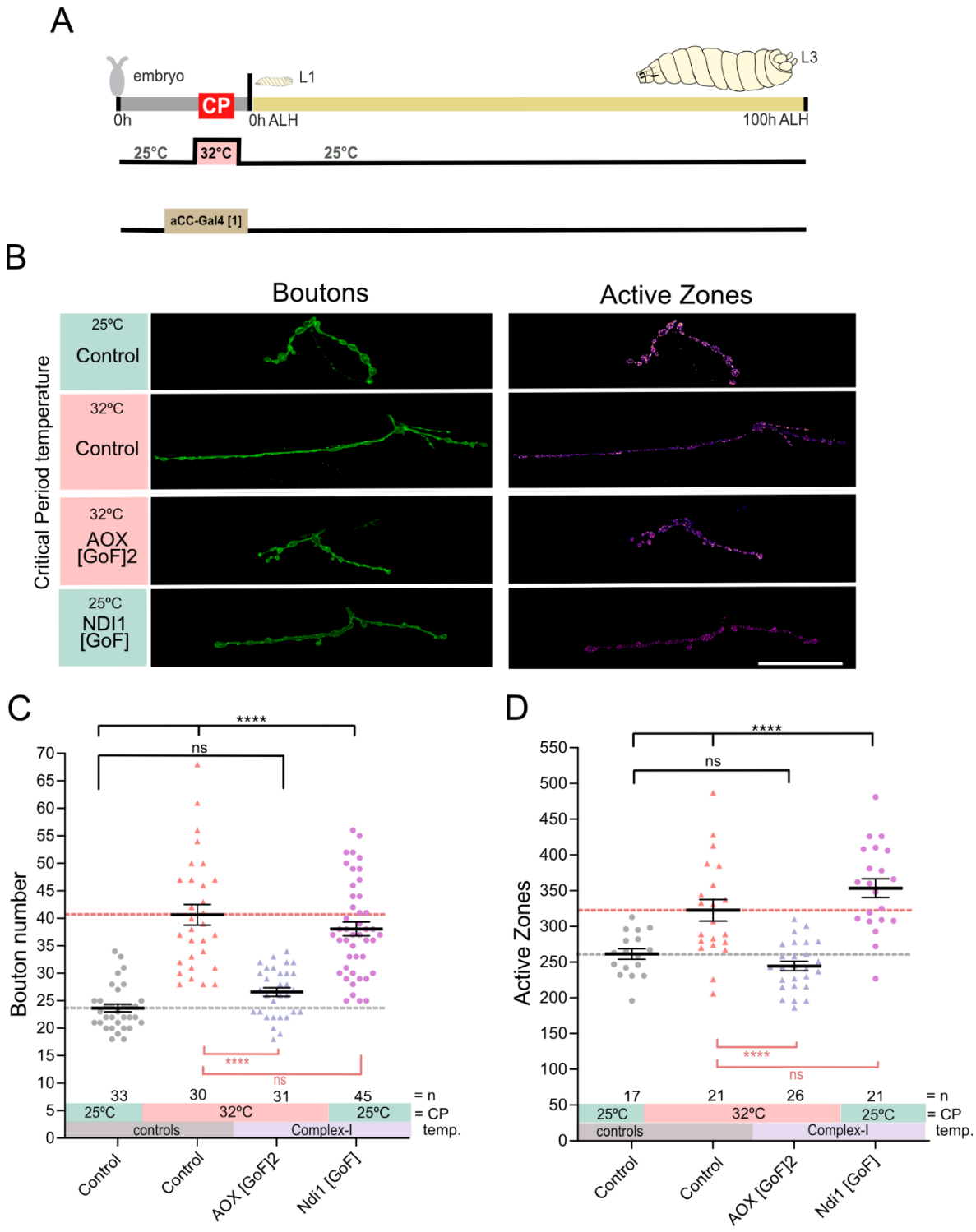
A
embryo
L1
L3
CP
0h
0h ALH
100h ALH
25°C
32°C
25°C
aCC-Gal4 [1]
B
Boutons
Active Zones
Critical Period temperature
25ºC
Control
32ºC
Control
32ºC
AOX
[GoF]2
25ºC
NDI1
[GoF]
C
Bouton number
****
ns
33
30
31
45
= n
25ºC
32ºC
25ºC
= CP
controls
Complex-I
temp.
Control
Control
AOX [GoF]2
Ndi1 [GoF]
D
Active Zones
17
21
26
21

Figure 4: HIF-1α is the signal downstream of ROS-RET.

A) Experimental paradigm

B) Representative images of aCC NMJ terminals on muscles DA1 in late wandering third instar larvae (100 hrs after larval hatching). Left: showing neuronal membrane, visualized with anti-HRP; centre: GluRIIA subunit; right: GluRIIB subunit, both displayed with lookup table "fire" to illustrate signal intensities (warmer colours indicating greater signal intensities). Temperature experienced during the embryonic critical period (25°C control *vs* 32°C heat stress) and simultaneous genetic manipulation of muscle DA1 during embryonic stages only. "Control" indicates control genotype heterozygous for Oregon-R and DA1-Gal4. Larvae were reared at the control temperature of 25°C until the late wandering stage, c. 100 hrs ALH Scale bar = 20 μm.

C) Dot-plot quantification shows changes to aCC NMJ growth on its target muscle DA1, based on the standard measure of the number of boutons (swellings containing multiple presynaptic release sites/active zones). Data are show with mean ± SEM, ANOVA, **** $p<0.00001$, 'ns' indicates statistical non-significance. Black asterisks indicate comparison with the control condition of 25°C throughout, genetically unmanipulated. Red asterisks indicate comparisons with control genotype exposed to 32°C heat stress during the embryonic critical period.

D) Dot-plot quantification shows changes in levels of the GluRIIA receptor subunit at aCC NMJs quantified in **C)**. Data are shown with mean ± SEM, ANOVA, * $p<0.01$, **** $p<0.00001$, 'ns' indicates statistical non-significance. Black asterisks indicate comparison with the control condition of 25°C throughout, genetically unmanipulated. Red asterisks indicate comparisons with control genotype exposed to 32°C heat stress during the embryonic critical period.

E) Dot-plot quantification as in **D)**, but for the low conductance GluRIIB receptor subunit, which remains unaffected by these manipulations.

A

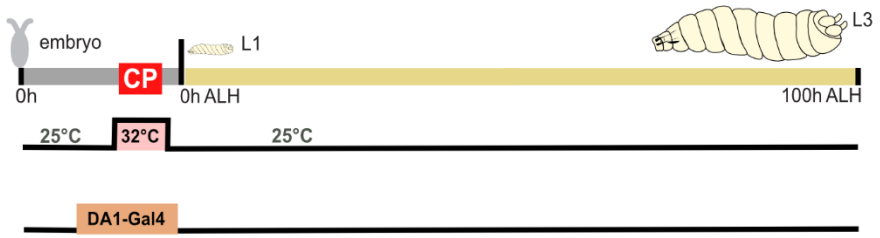
embryo
L1
L3
CP
0h
0h ALH
100h ALH
25°C
32°C
25°C
DA1-Gal4

B

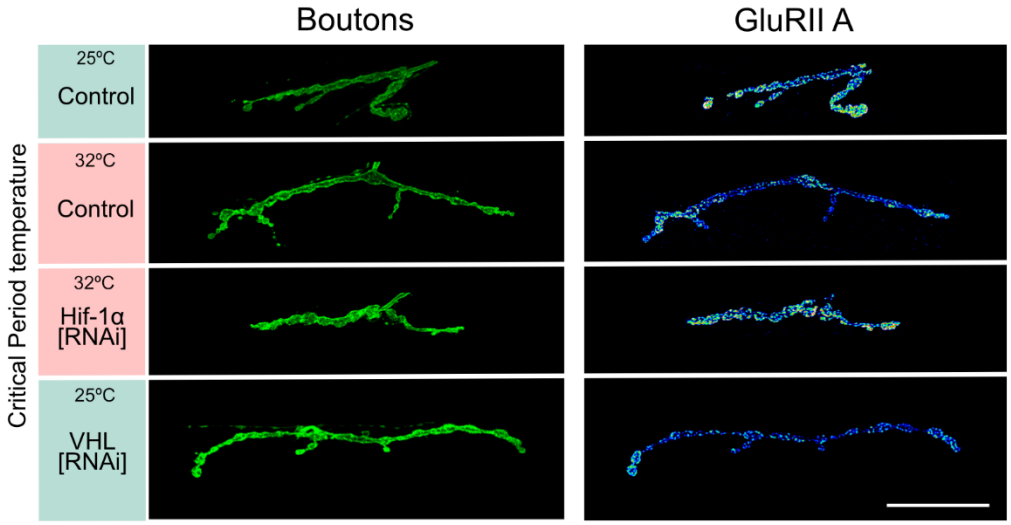
Boutons
GluRII A
Critical Period temperature
25ºC
Control
32ºC
Control
32ºC
Hif-1α
[RNAi]
25ºC
VHL
[RNAi]

C

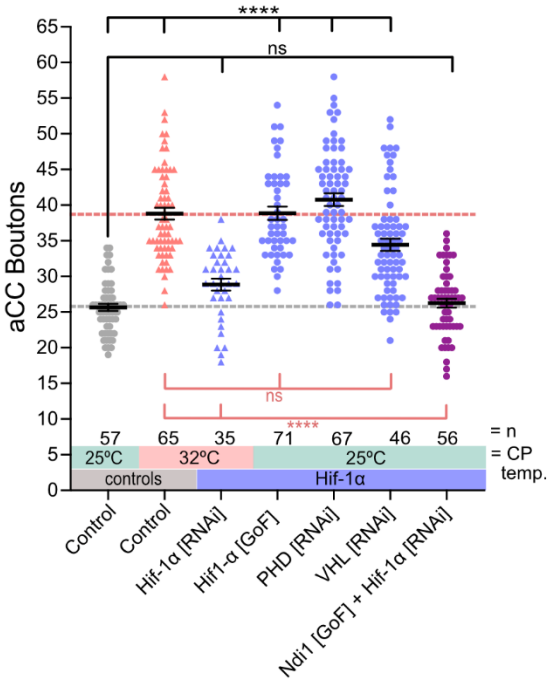
aCC Boutons
****
ns
ns
****
57 65 35 71 67 46 56
= n
25ºC 32ºC 25ºC
= CP temp.
controls
Hif-1α
Control
Control
Hif-1α [RNAi]
Hif1-α [GoF]
PHD [RNAi]
VHL [RNAi]
Ndi1 [GoF] + Hif-1α [RNAi]

D

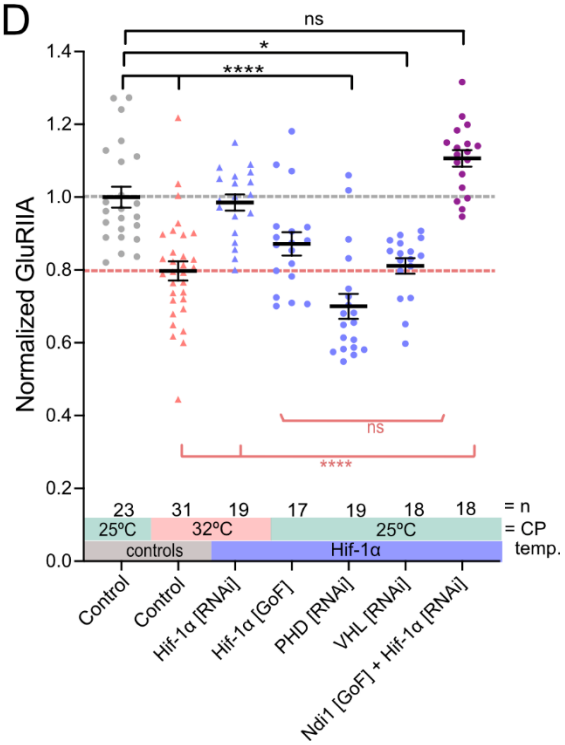
Normalized GluRIIA
ns
*
****
ns
****
23 31 19 17 19 18 18
= n
25ºC 32ºC 25ºC
= CP temp.
controls
Hif-1α
Control
Control
Hif-1α [RNAi]
Hif-1α [GoF]
PHD [RNAi]
VHL [RNAi]
Ndi1 [GoF] + Hif-1α [RNAi]

Figure 5. ROS by RET and HIF-1α signalling during the embryonic critical period are necessary and sufficient to induce a lasting changes to motoneuron excitability and crawling behaviour.

A) Experimental paradigm

B) aCC motoneuron excitability (i.e. action potential firing frequency triggered by current injected) at the late third instar larval stage. Temperature experienced during the embryonic critical period (25°C control *vs* 32°C heat stress) and simultaneous transient genetic manipulation of aCC motoneuron during embryonic stages, via aCC-Gal4 [1] (RN2-O-Gal4). "Control" indicates control genotype heterozygous for Oregon-R and aCC-Gal4 [1]. Larvae were reared at the control temperature of 25°C until the late wandering stage, c. 100 hrs ALH. Control at 25°C *vs* 32°C is significant at $p = 0.0005$; Control at 25°C *vs* HIF-1α[GoF] is significant at $p = 0.0015$; Control at 25°C *vs* AOX$[GoF]_2$ at 32°C is not significant at $p = 0.28$.

C) Cell capacitance measurements as indicators of cell size show no significant differences between aCC motoneurons from specimens in B).

D) Resting membrane potential, as an indicator for cell integrity, show no significant differences between aCC motoneurons from specimens in B).

E) Crawling speed of third instar larvae (72 hrs after larval hatching). Temperature experienced during the embryonic critical period (25°C control *vs* 32°C heat stress) and simultaneous genetic manipulation of all neurons during embryonic stages only. "Control" indicates control genotype heterozygous for Oregon-R and CNS-Gal4; Auxin-Gal80. Larvae were reared at the control temperature of 25°C until 72 hrs ALH. Each data point represents crawling speed from an individual uninterrupted continuous forward crawl, n = specimen replicate number, up to three crawls assayed for each larva. Mean ± SEM, ANOVA, ns = not significant, ****$p<0.00001$.

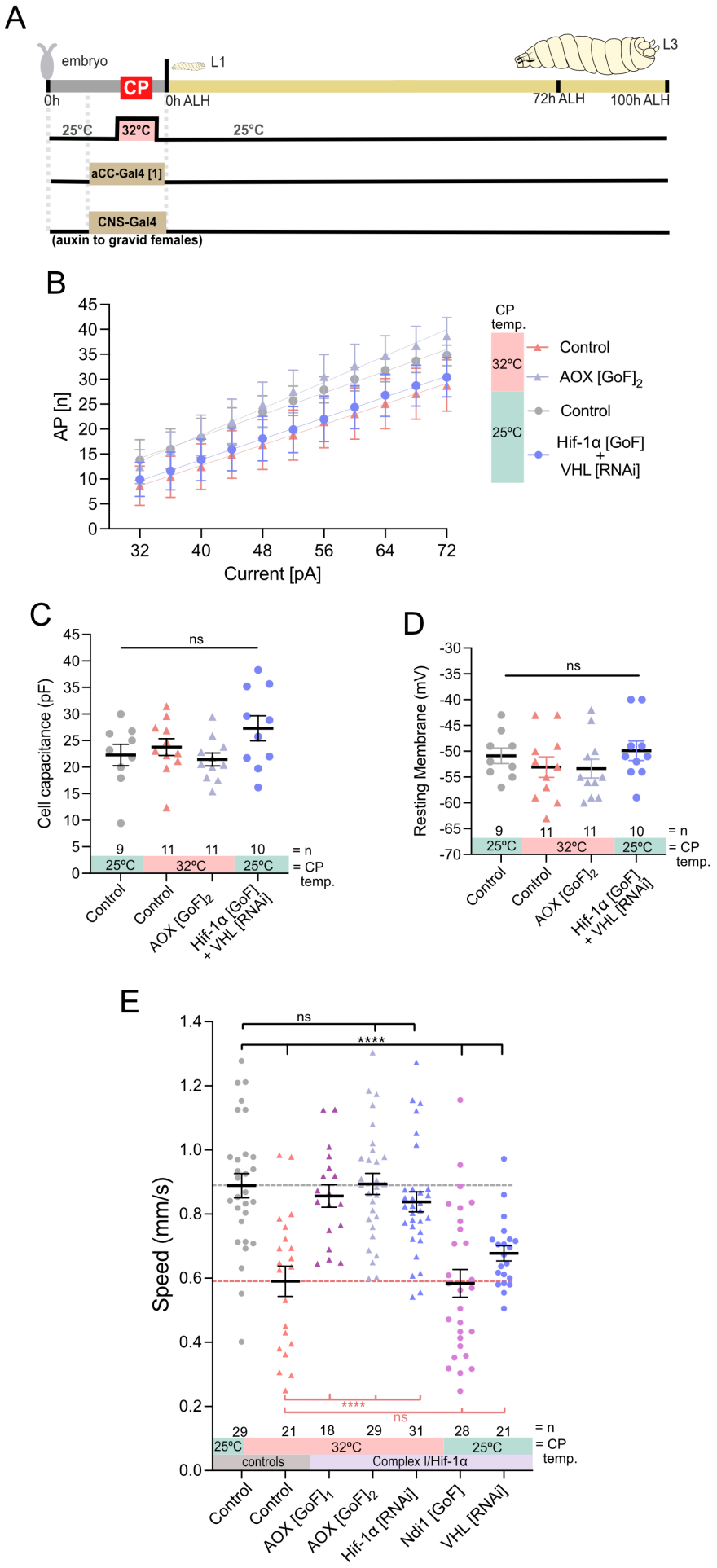
A
embryo
L1
L3
CP
0h
0h ALH
72h ALH
100h ALH
25°C
32°C
25°C
aCC-Gal4 [1]
CNS-Gal4
(auxin to gravid females)
B
AP [n]
Current [pA]
CP temp.
32°C
25°C
Control
AOX [GoF]2
Control
Hif-1α [GoF] + VHL [RNAi]
C
Cell capacitance (pF)
ns
9 11 11 10
= n
= CP temp.
Control
Control
AOX [GoF]2
Hif-1α [GoF] + VHL [RNAi]
D
Resting Membrane (mV)
ns
9 11 11 10
= n
= CP temp.
E
Speed (mm/s)
ns
****
29 21 18 29 31 28 21
= n
= CP temp.
controls
Complex I/Hif-1α
Control
Control
AOX [GoF]1
AOX [GoF]2
Hif-1α [RNAi]
Ndi1 [GoF]
VHL [RNAi]

Figure 6. Summary

A) Heat stress during the critical period induces ROS, which trigger *HIF-1α*, that is stabilised and thus accumulates in the nucleus, where it generates long-lasting changes that impact on **B)** NMJ development: larger presynaptic terminals and less GluRIIA, as well as behavioural phenotypes: reduction in both motoneuron excitability and crawling speed.

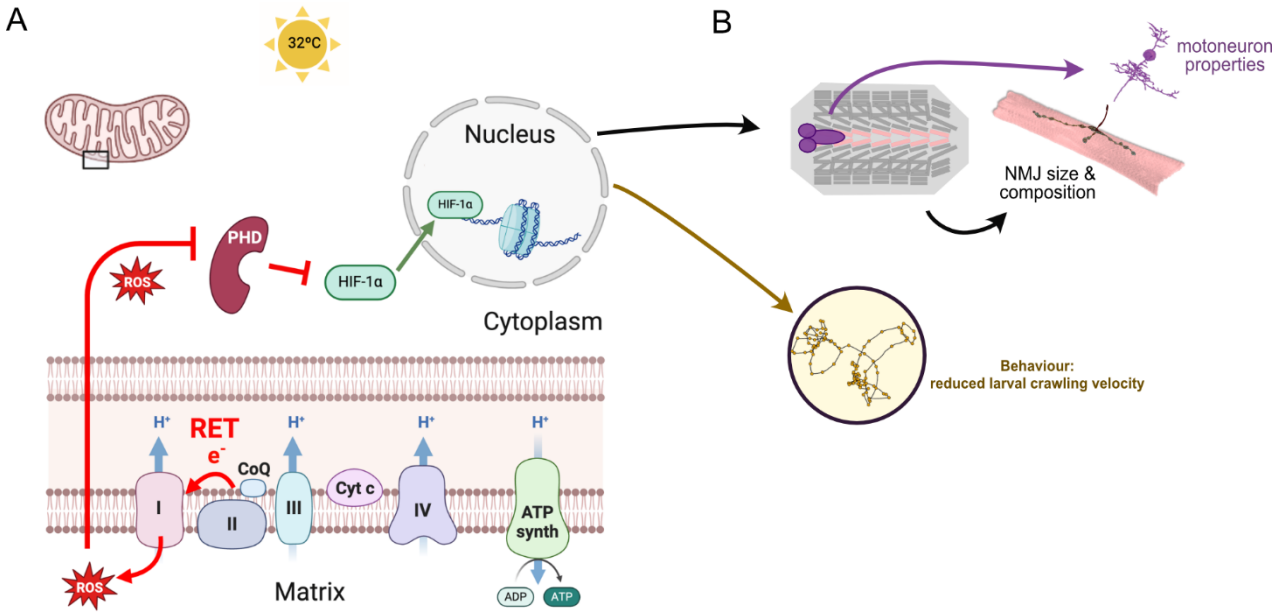

Tables

Table 1. Drosophila strains

Drosophila strain name	Additional information	Reference
Oregon-R-P2	Wild Type	Bloomington Drosophil Stock Center #2376
eve-Gal4eme (aka SS2-C-Gal4)	Gal4 expression targeted to muscle DA1 during embryonic stages only	Bataillé et al., 2010
aka RN2-O-gal4 (aCC-Gal4 [1])	Gal4 expression targeted to motorneurons aCC and RP2 during embryonic stages only	Fujioka et al., 2003
GMR94G06-Gal4 (aCC-Gal4 [2])	Gal4 expression targeted to motorneuron aCC	Pfeiffer et al., 2008; Liu et al., 2019; Bloomington Drosophil Stock Center #40701
GMR57C10-GAL4 (n-synaptobrevin-Gal4)	Gal4 expression targeted to neurons	Bloomington Drosophil Stock Center #39171
AtTIR1-T2A-AID-GAL80-AID (Auxin-gal80)	Ubiquitously express GAL80 sensitive to auxin	(McClure et al., 2022); gift from Tony Southall
UAS-mito-catalase	Mitochondrial targeted catalase under UAS control	Kwong et al., 2000; gift from Alex Whitworth
UAS-Prx3	Peroxiredoxin 3 under UAS control	gift from Alberto Sanz
UAS-ND75 [RNAi]	Expresses dsRNA for RNAi of ND75 (FBgn0017566) under UAS control	Vienna Drosophila Resource Center #100733/KK; gift from Alberto Sanz
UAS-AOX [GoF]1	Expresses AOX from C. intestinalis under UAS control (allele F6)	Fernandez-Ayala et al., 2009; gift from Alberto Sanz
UAS-AOX [GoF]2	Expresses AOX from C. intestinalis under UAS control (allele F24)	Fernandez-Ayala et al., 2009; gift from Alberto Sanz
UAS-Ndi1 [GoF]	Expresses Ndi1 from S.cerevisae under UAS control (allele A46 and B20)	Sanz et al., 2010; gift from Alberto Sanz
UAS-Sima [RNAi]	Expresses dsRNA for RNAi of sima (FBgn0266411) under UAS control	Bloomington Drosophil Stock Center #26207
UAS-Sima [GoF]	Expresses sima (FBgn0266411) under UAS control	Gift from Joe Bateman
UAS-VHL [RNAi]	Expresses dsRNA for RNAi of VHL (FBgn0041174) under UAS control	Bloomington Drosophil Stock Center #50727
UAS-PHD [RNAi]	Expresses dsRNA for RNAi of PHD (FBgn0264785) under UAS control	Bloomington Drosophil Stock Center #34717

Author Contributions

Conceptualization: D.S.-C. and M.L; Investigation: D.S.-C. and B.C.; Writing – Original Draft: D.S.-C. and M.L; Writing – Review & Editing: D.S.-C., B.C, M.C.W.O., T.P., R.A.B. and M.L.; Supervision: R.A.B and M.L.; Funding Acquisition: D.S-C., R.A.B and M.L.

Author competing interests

The authors declare no competing interests.

Funding

D.S.-C. was supported by the European Molecular Biology Organization (EMBO) with a long-term EMBO fellowship (ALTF 62-2021). This work was supported by a Joint Wellcome Trust Investigator Award to R.A.B. and M.L. (217099/Z/19/Z).

Acknowledgments

The authors are grateful to Mihaela Serpe for the Rabbit polyclonal anti-GluRIIB antiserum. The authors are grateful to Tony Southall, Alex Whitworth, Joe Bateman, Alberto Sanz, as well as the Bloomington Drosophila Stock Center and Vienna Drosophila Resource Center for generously providing fly stocks. The work benefited from the Imaging Facility, Department of Zoology, supported by Matt Wayland and Tom Pettini, and funds from a

Wellcome Trust Equipment Grant (WT079204) with contributions by the Sir Isaac Newton Trust in Cambridge, including Research Grant [18.07ii(c)]. Work on this project benefited from the Manchester Fly Facility, established through funds from the University of Manchester and the Wellcome Trust (Grant 087742/Z/08/Z).

Supplementary Material

Supplementary figure 1.

A) Experimental paradigm

B) Representative images of aCC NMJ terminals on muscles DA1 in late wandering third instar larvae (100 hrs after larval hatching). Left: showing neuronal membrane, visualized with anti-HRP; right: active zones (α-BRP staining). Genetic manipulation of motoneuron aCC during the critical period *vs* after critical period closure. "Control" indicates control genotype heterozygous for Oregon-R and aCC-Gal4[2]; Auxin-Gal80. Larvae were reared at the control temperature of 25°C until the late wandering stage, c. 100 hrs ALH. Scale bar = 20 μm.

C) Dot-plot quantification shows changes to aCC NMJ growth on its target muscle DA1, based on the standard measure of the number of boutons (swellings containing multiple presynaptic release sites/active zones). Data are show with mean ± SEM, ANOVA, **** $p<0.00001$, 'ns' indicates statistical non-significance.

D) Dot-plot quantification shows changes in number of the active zones at aCC NMJs quantified in C). Data are shown with mean ± SEM, ANOVA, *** $p<0.0001$, **** $p<0.00001$, 'ns' indicates statistical non-significance.

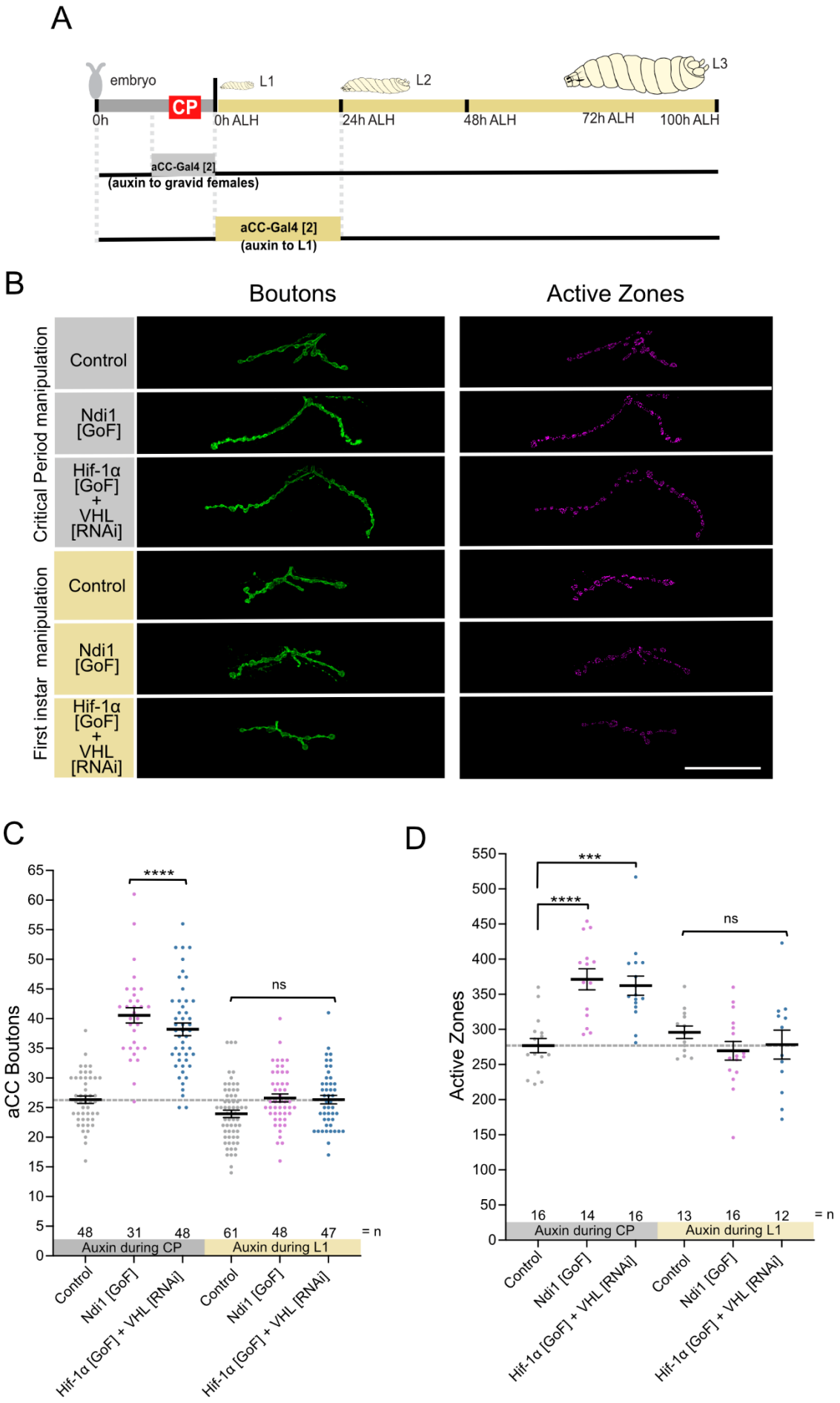
A
embryo
L1
L2
L3
CP
0h
0h ALH
24h ALH
48h ALH
72h ALH
100h ALH
aCC-Gal4 [2]
(auxin to gravid females)
aCC-Gal4 [2]
(auxin to L1)
B
Boutons
Active Zones
Critical Period manipulation
First instar manipulation
Control
Ndi1 [GoF]
Hif-1α [GoF] + VHL [RNAi]
Control
Ndi1 [GoF]
Hif-1α [GoF] + VHL [RNAi]
C
aCC Boutons
****
ns
48 31 48 61 48 47 = n
Auxin during CP
Auxin during L1
Control
Ndi1 [GoF]
Hif-1α [GoF] + VHL [RNAi]
Control
Ndi1 [GoF]
Hif-1α [GoF] + VHL [RNAi]
D
Active Zones
***
****
ns
16 14 16 13 16 12 = n
Auxin during CP
Auxin during L1
Control
Ndi1 [GoF]
Hif-1α [GoF] + VHL [RNAi]
Control
Ndi1 [GoF]
Hif-1α [GoF] + VHL [RNAi]

Supplementary figure 2.

A) Experimental paradigm
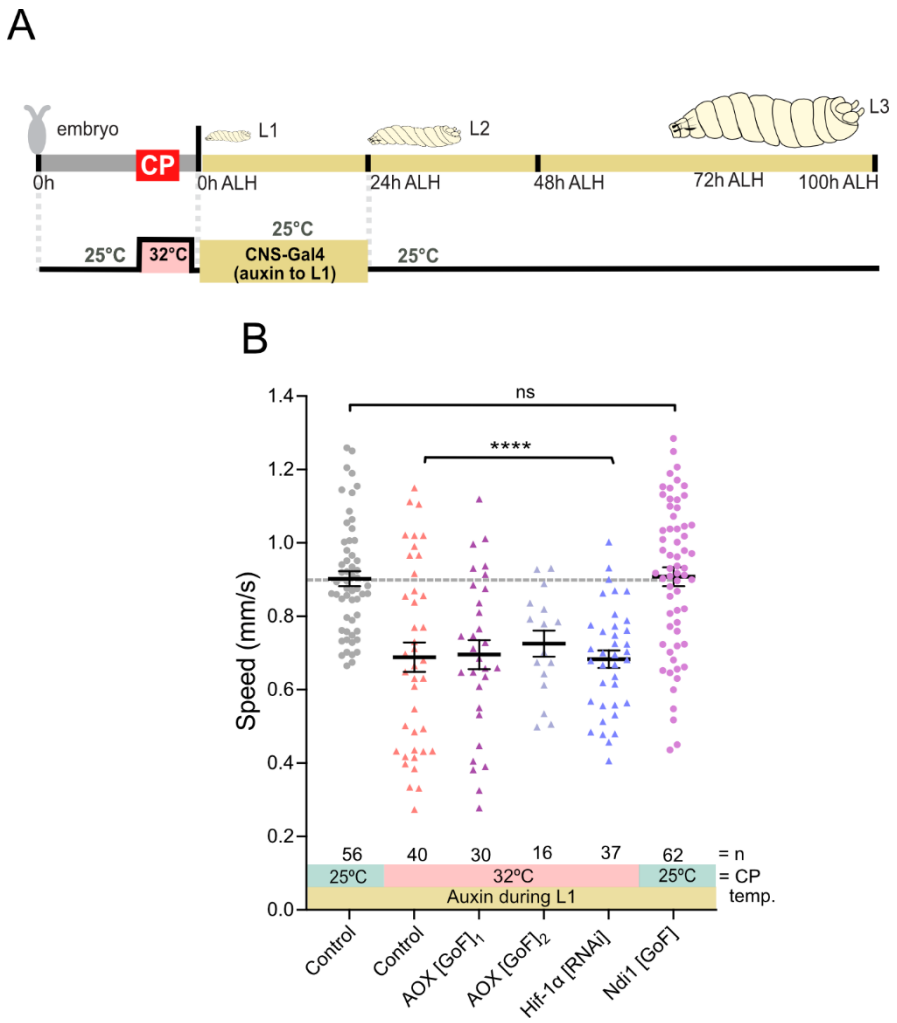
B) Crawling speed of third instar larvae (72 hrs after larval hatching). Temperature experienced during the embryonic critical period (25°C control *vs* 32°C heat stress) and simultaneous genetic manipulation of all neurons during first instar stage. "Control" indicates control genotype heterozygous for Oregon-R and CNS-Gal4; Auxin-Gal80. Larvae were reared at the control temperature of 25°C until 72 hrs ALH. Each data point represents crawling speed from an individual uninterrupted continuous forward crawl, n = specimen replicate number, up to three crawls assayed for each larva. Mean ± SEM, ANOVA, ns = not significant, ****p<0.00001.